E-9675

NASA Technical Publication 3555

Demonstration of Wavelet Techniques in the Spectral Analysis of Bypass Transition Data

Jacques Lewalle
Syracuse University

David E. Ashpis
Lewis Research Center, Cleveland, Ohio

Ki-Hyeon Sohn
University of Toledo

December 1997

The NASA STI Program Office . . . in Profile

Since its founding, NASA has been dedicated to the advancement of aeronautics and space science. The NASA Scientific and Technical Information (STI) Program Office plays a key part in helping NASA maintain this important role.

The NASA STI Program Office is operated by Langley Research Center, the Lead Center for NASA's scientific and technical information. The NASA STI Program Office provides access to the NASA STI Database, the largest collection of aeronautical and space science STI in the world. The Program Office is also NASA's institutional mechanism for disseminating the results of its research and development activities. These results are published by NASA in the NASA STI Report Series, which includes the following report types:

- TECHNICAL PUBLICATION. Reports of completed research or a major significant phase of research that present the results of NASA programs and include extensive data or theoretical analysis. Includes compilations of significant scientific and technical data and information deemed to be of continuing reference value. NASA's counterpart of peer-reviewed formal professional papers but has less stringent limitations on manuscript length and extent of graphic presentations.

- TECHNICAL MEMORANDUM. Scientific and technical findings that are preliminary or of specialized interest, e.g., quick release reports, working papers, and bibliographies that contain minimal annotation. Does not contain extensive analysis.

- CONTRACTOR REPORT. Scientific and technical findings by NASA-sponsored contractors and grantees.

- CONFERENCE PUBLICATION. Collected papers from scientific and technical conferences, symposia, seminars, or other meetings sponsored or cosponsored by NASA.

- SPECIAL PUBLICATION. Scientific, technical, or historical information from NASA programs, projects, and missions, often concerned with subjects having substantial public interest.

- TECHNICAL TRANSLATION. English-language translations of foreign scientific and technical material pertinent to NASA's mission.

Specialized services that complement the STI Program Office's diverse offerings include creating custom thesauri, building customized data bases, organizing and publishing research results . . . even providing videos.

For more information about the NASA STI Program Office, see the following:

- Access the NASA STI Program Home Page at ***http://www.sti.nasa.gov***

- E-mail your question via the Internet to help@sti.nasa.gov

- Fax your question to the NASA Access Help Desk at (301) 621-0134

- Telephone the NASA Access Help Desk at (301) 621-0390

- Write to:
  NASA Access Help Desk
  NASA Center for AeroSpace Information
  800 Elkridge Landing Road
  Linthicum Heights, MD 21090-2934

NASA Technical Publication 3555

Demonstration of Wavelet Techniques in the Spectral Analysis of Bypass Transition Data

Jacques Lewalle
Syracuse University

David E. Ashpis
Lewis Research Center, Cleveland, Ohio

Ki-Hyeon Sohn
University of Toledo

National Aeronautics and
Space Administration

Lewis Research Center

December 1997

Acknowledgments

This work was performed as part of the Multiresolution Analysis Project (Dr. Dzu K. Le, Principal Investigator) and was supported by the NASA Lewis Research Center Director's Discretionary Fund.

Available from

NASA Center for Aerospace Information
800 Elkridge Landing Road
Linthicum Heights, MD 21090-2934
Price Code: A03

National Technical Information Service
5287 Port Royal Road
Springfield, VA 22100
Price Code: A03

Demonstration of Wavelet Techniques in the Spectral Analysis of Bypass Transition Data

Jacques Lewalle
Syracuse University
Syracuse, New York 13244

David E. Ashpis
National Aeronautics and Space Administration
Lewis Research Center
Cleveland, Ohio 44135

Ki-Hyeon Sohn
University of Toledo
Toledo, Ohio 43606

Summary

A number of wavelet-based techniques for the analysis of experimental data are developed and illustrated. A multiscale analysis based on the Mexican hat wavelet is demonstrated as a tool for acquiring physical and quantitative information not obtainable by standard signal analysis methods. Experimental data for the analysis came from simultaneous hot-wire velocity traces in a bypass transition of the boundary layer on a heated flat plate. A pair of traces (two components of velocity) at one location was excerpted. A number of ensemble and conditional statistics related to dominant time scales for energy and momentum transport were calculated. The analysis revealed a lack of energy-dominant time scales inside turbulent spots but identified transport-dominant scales inside spots that account for the largest part of the Reynolds stress. Momentum transport was much more intermittent than were energetic fluctuations. This work is the first step in a continuing study of the spatial evolution of these scale-related statistics, the goal being to apply the multiscale analysis results to improve the modeling of transitional and turbulent industrial flows.

Introduction

The traditional tools of signal analysis (ref. 1) work either in the time domain, where sequential information is available at the exclusion of spectral information, or in the frequency domain, where the Fourier-transformed signal conceals the time of occurrence and provides purely spectral information. Spectral analysis is essential to describe complex phenomena and to understand their dynamics; hence, running data through a Fast Fourier transform (FFT) analyzer is a standard procedure. A Fourier analysis is an attempt to match infinite sinusoidal wave trains with the data. Although this approach is rewarding and fundamentally justified when periodic components are expected in the signal, it fails to describe the complexity of the system when broadband spectra are obtained. For example, the infinite repetition of the sine wave in Fourier analysis is a poor match for the intermittency or modulation of velocity traces in high Reynolds number flows. Wavelet transforms provide an alternative with a localized waveform. Wavelet methods have evolved over the past few years as a versatile substitute for earlier time-frequency approaches (refs. 2 to 4).

Practical Relevance of Bypass Transition Study

In this study, wavelet techniques were used to analyze the multiscale content of one pair of u-v velocity traces from the data of Sohn and Reshotko (ref. 5). This report identifies, demonstrates, and discusses the combination of procedures that yield information (unavailable by other means) about the energy spectra, momentum transport, and the flow structure inside and between turbulent spots. This study complements the work of Sohn, Zaman, and Reshotko (refs. 5 and 6) in documenting a basic flow that includes some of the complex dynamics of turbomachinery and other industrial flows.

The sequence of events leading to boundary layer transition in laminar flows is well understood (ref. 7). However, free-stream conditions in turbomachinery are practically never laminar. If strong enough, the free-stream turbulence can induce nonlinear perturbations in the boundary layer that bypass the linear sequence of Tollmien-Schlichting waves and their three-dimensional nonlinear offspring, leading to the development of turbulent spots.

In bypass transition (ref. 8), the sudden appearance of spots and their rapid growth have been measured in some detail. The effects of isolated disturbances (ref. 9) and statistically steady

grid turbulence have been documented in a number of papers (refs.10 to 14). The complexity of the problem increases in turbomachinery because of the unsteadiness of the ambient turbulence associated with wake passing (refs. 15 and 16). For engineering applications (e.g., in gas turbine design), modeling the friction and heat transfer in the transition region is an open problem, and the importance of improving the modeling of these phenomena has been recognized in the work of others (refs. 17 to 21). The physical content of practical models could be improved with a better understanding of the active scales of motion and their evolution in the transition region.

Bypass transition combines the characteristics of the free-stream turbulence with those of the turbulent spots generated in the boundary layer. Separating the multiple scales involved in this process is important in understanding the physical phenomena and in improving the computational models based on them. However, the intermittent nature of the flow field has prevented the effective use of the conventional methods of spectral analysis of experimental data. Therefore, the advantages of wavelet analysis over Fourier analysis are illustrated in this report.

The Data

The experimental data analyzed herein were collected by Sohn and Reshotko whose work is documented in reference 5 and will not be reproduced here. The flow of interest is the developing boundary layer on a heated flat plate. Free-stream turbulence was generated by one of several grids so that different turbulence length scales and intensity levels (in the range of 0.5 to 6.5 percent) could be achieved. A three-wire miniature probe was used to collect simultaneous records (32 768 points) of streamwise and transverse velocities and temperature at a sampling rate of 50 kHz. Some of these time traces were saved for streamwise locations ranging from 9 to 20 in. from the leading edge, corresponding to Re_θ (Reynolds numbers based on momentum thickness) of 470 to 1580. This study used data collected for the grid 1 case (with a nominal 1.1-percent free-stream turbulence level (ref. 5)) at a point $X = 9$ in. ($Re_\theta = 470$). Although this point is in the early transition range, a Tollmien-Schlichting spike occurring at $X = 5$ in. in the Fourier power spectra is no longer visible at $X = 7$ in. and beyond (ref. 5). The nominal distance to the wall $Y = 0.030$ in. ($Y/\theta \sim 3.0$) is within the range where reasonably energetic spots are suitable for the illustrations presented herein. In a subsequent report, the methods demonstrated will be applied to calculate the spatial variations of the statistics in the transverse and streamwise directions.

Symbols

$E(\kappa)$	wavelet power spectrum
$f(t)$	signal
$f_g, f_g(\kappa,t)$	wavelet transform
$f_2(\kappa,t)$	wavelet transform of f(t) with g_2 wavelet
$g(t)$	wavelet
g_n	Gaussian wavelet of order n
g_2	Mexican hat wavelet (Gaussian wavelet of order 2)
$\bar{I}$	intermittency factor
$I(t)$	indicator function
Re_θ	Reynolds number based on momentum thickness
t	time
t^*	dimensionless time
$u(t),u$	streamwise velocity
$v(t),v$	normal velocity
$U_n(\kappa,t)$	defined by eq. (13) for u_{2n}
$u_n(\kappa,t)$	wavelet transform of $u(t)$ with wavelet g_n (eq. (12))
$u_2(\kappa,t)$	g_2 wavelet map
$V_n(\kappa,t)$	defined by eq. (13) for v_{2n}
$\Gamma(n)$	gamma function
θ	momentum thickness
κ	inverse duration
κ_u	inverse duration of u
κ_v	inverse duration of v
κ^{-1}	duration of wavelet
τ	time integration parameter
τ_R	Reynolds stress (eq. (11))
ϕ	frequency

Subscripts:

I	turbulent conditioned
n	order of Gaussian wavelet
1-I	nonturbulent conditioned

Wavelet Transforms

The advantage of wavelet methods over conventional techniques of spectral analysis is the ease with which local spectral contributions (to energy, transport, or other properties of interest) can be isolated, screened according to various criteria, and combined into conditional statistics. After a brief introduction to wavelet transforms, several wavelet tools will be described, the algorithms elucidated, and the results illustrated. Because the results are quantitative, they will be interpreted from a dynamical perspective.

Basic Formulas

From the expanding body of literature on applied wavelet techniques, only applications to fluid mechanics will be cited. Details and alternative methods applied to experimental data can be found in references 16 and 22 to 27. Turbulence direct numerical simulation (DNS) data were also treated in references 3, 28, and 29. The collection of wavelets considered in this study was limited to one type, the Mexican hat, but its value is enhanced by the subsequent processing for selective feature enhancement and statistical relevance. The work will concern continuous wavelets because the presentation will be simpler. As dictated by the data, the actual implementation of the formulas is in discretized form.

A wavelet $g(t)$ is a function that meets the acceptability criterion (ref. 2): for a real wavelet, it is sufficient that the integral over the entire time axis vanish. Practically, one wants to combine a degree of localization in time with localization in the frequency domain. The wavelet transform f_g of a signal $f(t)$ is obtained by convolving the signal with the wavelet and repeating this process for a range of wavelet durations. Analytically,

$$f_g(\kappa,t) = \int_{-\infty}^{\infty} \kappa^{1/2} f(\tau) g^*\left[\kappa(\tau - t)\right] \mathrm{d}\tau \qquad (1)$$

where the asterisk denotes complex conjugation and τ is the integration parameter representing the translation of the wavelet. The localization of the wavelet is governed by the variable t and its duration by κ^{-1}. Although the integration is nominally over the entire time axis, only the neighborhood of the center of the wavelet will contribute significantly to the integral. The factor $\kappa^{1/2}$ is arbitrary (Wang, Q.; Brasseur, J.G.; Smith, R.W.; Smits, A.J.: Multi-Dimensional Continuous Wavelet Transforms and Applications to Turbulence Data. Unpublished report, 1994) and is chosen here for convenience in the Parseval theorem (see Energy Maps section). The magnitude of the wavelet transform $f_g(\kappa,t)$ reflects the manner in which the shape of the wavelet matches the local shape of the signal.

Wavelet Selection

The wavelet literature contains references to a large number of wavelets, variously recommended for their optimal properties or specialized ability to resonate with the data. The wavelet selection made herein was governed by flexibility and ease of implementation and interpretation. A wavelet is characterized by three attributes: shape, duration, and location in time relative to the data. Time and duration become the two independent variables, as seen in equation (1). Shape is the dominant degree of freedom, affecting the eventual interpretation of results and the balance that is actually achieved between spectral and temporal resolution.

From the Gaussian family of wavelets of order n,

$$g_n(t^*) = (-1)^n \frac{\mathrm{d}^n}{\mathrm{d}t^n} \mathrm{e}^{-t^{*2}/2} \qquad (2)$$

the Mexican hat wavelet g_2 (fig. 1) was chosen:

$$g_2\left(t^*\right) = \left(t^{*2} - 1\right)\mathrm{e}^{-t^{*2}/2} \qquad (3)$$

In the following, a wavelet transform of variables with the g_2 wavelet will be designated by the subscript 2. The two reasons for this choice are that (1) it is easy (two integrations by parts) to show that the wavelet transform with g_2 is equivalent to the smoothing of the signal with a Gaussian filter followed by multiplication by a scale-dependent factor and double differentiation with respect to time. Thus, the g_2 transform will identify maxima and minima of the smoothed signal. (2) The scale resolution of the turbulent transport (see the sections from Correlation Maps to Higher Order Correlations) is greatly simplified by the fast-inverse formula (developed in ref. 30), which applies only to g_2 and to higher order Gaussian wavelets of even order.

The use of Morlet wavelets (ref. 2) to identify periodic wave trains (and other specialized waveforms) will be attempted in the future.

Duration and Frequency

Strictly speaking, frequency is a concept applicable only to periodic phenomena. Even with respect to broadband signals, repetition is implied by the decomposition into a Fourier wave train. However, the emphasis must sometimes be placed on

individual events for which the concept of frequency is confusing and inappropriate. Although the duration of the event is the better concept in this context, there is merit in relying on familiar terminology and numerical values. Thus, the terms "duration" κ^{-1} and "frequency" ϕ will be used herein and their corresponding values given now. The correspondence between duration and frequency can be calculated exactly for a cosine signal $f(t) = \cos(2\pi\phi t)$ for which the g_2 wavelet transform is

$$f_2(\kappa,t) = -\sqrt{(2\pi)}(2\pi\phi)^2 \cos(2\pi\phi t)\kappa^{(-5/2)} \exp\left(\frac{-2\pi^2\phi^2}{\kappa^2}\right) \quad (4)$$

The duration κ^{-1} corresponding to the largest values of this wavelet transform is given by

$$\frac{\phi}{\kappa} = \frac{\sqrt{2.5}}{2\pi} = 0.2516 \quad (5)$$

This relation was used successfully with broadband signals in reference 23. The dependency of duration on wavelet shape is discussed in more detail in reference 31. The conversion factor of 0.2516 is applicable only to the Mexican hat wavelet. With this limitation, the correspondence is

$$1 \text{ kHz} \leftrightarrow 0.2516 \text{ ms} \quad 1 \text{ ms} \leftrightarrow 0.2516 \text{ kHz} \quad (6)$$

A Wavelet Map

In this study, the wavelet transform (eq. (1)) of each signal is the first step in implementing all algorithms. Over the range of times and durations selected, the wavelet coefficients (the values of the transform) are computed as arrays of numbers. The resulting "wavelet map" is the color-coded plots of these coefficients in the plane of time and duration. A short sample will be used to illustrate this concept.

Figure 2 shows a portion of a streamwise velocity trace $u(t)$ and the corresponding wavelet map $u_2(\kappa, t)$. The presence of the turbulent spot is obvious from the raw data and is delineated by dotted lines t_1,t_2. This part of the raw signal is referred to as the spot or the turbulent part. The fluctuations outside the spot are essentially laminar and are attributed to the footprints of the free-stream turbulence and/or to the spot-induced motion in the boundary layer. These nonspot segments of the signal are sometimes called "laminarlike" or "pseudolaminar," but we will refer to them as the nonturbulent part.

The wavelet map describes the temporal relationship existing in the various flow events of different sizes and quantifies its magnitude. The time axis is common to the raw data and to the abscissa of the wavelet map; the ordinate is usually logarithmic, and short durations (equivalent to high frequency) are plotted at the bottom of the map. The wavelet coefficients (discretized values of u_2) are color coded and appear as contour lines. With signal features sorted by duration, time of occurrence, and magnitude, a quantitative picture emerges for the succession of features at a given duration (along a horizontal line) or for the simultaneous presence of features of different durations (vertical line). For example, in the band of durations of 0.3 to 2 ms (0.84 to 0.13 kHz) delineated by solid lines a_1,a_2, random but apparently homogeneous fluctuations are seen and are attributed to the footprints of the free-stream turbulence. The small-scale activity (around 0.1 ms or 2.52 kHz) in the lower part of the figure is limited to a spot located at 12 ms of this particular sample. Also seen is the local drop in mean velocity inside the spot (a relatively long-duration section of the horizontal line a_1 between the dotted lines). This drop is associated with the three largest values of the wavelet transform and corresponds to the projection of the lower velocities on the first maximum, minimum, and second maximum of the Mexican hat wavelet, respectively. The following sections will present several criteria used to select some features from wavelet maps. If necessary, these features will be enhanced so that statistics can be constructed from these events.

Focus on Energy

Energy Maps

One of the principal analytical results obtained for continuous wavelet transforms concerns the temporal/spectral distribution of energy. As in the case of the Fourier power spectrum, the formulas originate from Parseval's theorem (ref. 2). Thus, for the first two Gaussian wavelets,

$$\int_{-\infty}^{\infty} |f(t)|^2 \, dt = \frac{1}{\pi}\int_0^{\infty} d\kappa \int_{-\infty}^{\infty} dt \left|f_g(\kappa,t)\right|^2$$

$$= \int_0^{\infty} 2E(\kappa)\, d\kappa \quad (7)$$

by which the expression $|f_g(\kappa,t)|^2/\pi$ can be interpreted as the local energy spectral density. When this energy density is color coded in the plane of time and duration, it is called an energy map. Figure 3 is an energy map (in logarithmic color scale) that corresponds to the data in figure 2.

The information in the wavelet and energy maps comprises every local maximum and minimum of the signal. The identification of a multitude of individual energy maxima at different durations enables the selection of the most significant events. However, the description of each event individually is an endless and fruitless task. The most useful applications of wavelet transforms in the data analysis are those that reduce the amount of information required to extract meaningful statistics. A few applications will be presented next.

In the case of figure 3, a useful procedure (ref. 24) is to smooth each constant line κ of the map with a Gaussian filter of a matching duration:

$$\tilde{f}_g^2(\kappa,t) = \int_{-\infty}^{\infty} f_g^2(\kappa,\tau)\frac{\kappa}{\sqrt{2\pi}}\exp\left[-\frac{\kappa^2(\tau-t)^2}{2}\right]\mathrm{d}\,\tau \qquad (8)$$

Then, normalize each line (fixed κ) so that it has unit variance. The result of smoothing and normalizing the energy map is shown in figure 4, from which a number of observations can be made. (1) The plot is drastically simplified, as intended. (2) The leading and trailing edges of the spot can be identified over a range of scales extending over more than a decade (delineated by thick, solid contour lines labeled *A*). (3) The small-scale activity is not homogeneously distributed inside the spot but appears to be structured as pulses. (4) A band of weak, intermittent activity associated with the nonturbulent part (labeled *B*) is noted in the 0.2- to 0.5-ms (1.26- to 0.5-kHz) range. It may be coincidental that this range brackets the frequency (0.9-kHz or 0.28-ms duration) of the Tollmien-Schlichting waves observed upstream of the present location (ref 5). Inspection of this segment of velocity signal reveals little evidence of periodic oscillations, except for perhaps a few periods at the trailing edge of the spot. However, no such wave trains are visible on the matching transverse velocity trace. This feature, if confirmed, will be the object of subsequent studies.

Mean Power Spectra and Energetic Scales

From the energy map (fig. 3) and the Parseval relation (eq. (7)), it is clear that a time integration of the energy map will yield a distribution of energy $E(\kappa)$ akin to the Fourier power spectral density (refs. 23 and 24). A direct comparison of the two spectra is presented in figure 5, in which the duration has been converted to the equivalent frequency with the aid of equation (5). Consistent with the interpretation of the wavelet transform as a bandpass filter (Wang, Q.; Brasseur, J.G.; Smith, R.W.; Smits, A.J.: Multi-Dimensional Continuous Wavelet Transforms and Applications to Turbulence Data. Unpublished report, 1994), the wavelet spectrum is considerably smoother than its Fourier counterpart. It was verified that the factor of the order of 2 separating the two spectra is compensated for at the very low frequencies so that both power spectra integrate to the total energy of the signal. The spectra are generally featureless, which is in agreement with the results of reference 5.

The spectral energy content in a frequency band around κ is estimated by the integral

$$\Delta E(\kappa) = \int E(\kappa)\,\mathrm{d}\,\kappa = \int \kappa E(\kappa)\,\mathrm{d}(\log\kappa) \qquad (9)$$

A spectral range in the vicinity of a given duration is best specified on the logarithmic scale; indeed, on a linear scale, the energy density per unit frequency generally exhibits no dominant scales except at infinite duration. By contrast, on a logarithmic scale, the energy density per octave de-emphasizes the longest durations, and the presence of a maximum can serve as the basis for a definition of dominant scales. Accordingly, energetically dominant scales are identified as the maximum of $\kappa E(\kappa)$, as shown in figure 6. Also seen is that the energy has a strong peak at about 1.26 ms (0.2 kHz).

The spots are easily identified on the energy maps of figures 3 and 4 at all durations shorter than 0.3 ms (frequencies higher than 0.84 kHz). Their failure to have a dominant scale signature in figure 6 could be attributed to the relatively small fraction of time during which the spots are present (termed the intermittency factor). The following subsection addresses the need for conditional sampling.

Laminar-Turbulent Discrimination and Conditional Spectra

The need to differentiate the contributions of nonturbulent (nominally laminar) from turbulent portions of a signal in intermittent flows is well known. This differentiation is based on small-scale fluctuations present within the turbulent patches. Hedley and Keffer (ref. 32) surveyed a number of options and issued recommendations for the discrimination algorithms. Variants were later suggested by Antonia (ref. 33). Applications to bypass transition can be found in references 5 and 34, and some of the steps used in this study are summarized.

A signal such as the u-trace shown in figure 2 contains the information necessary for making laminar-turbulent decisions and is termed a discriminator signal. Turbulent spots can be identified by the presence of small-scale fluctuations (fig. 4) that, for best results, are enhanced by differentiating the discriminator signal. Squaring eliminates irrelevant sign information and results in a detector function. Smoothing over scales of the order of the Taylor microscale fills the gaps between the small-scale patches, yielding the criterion function. This criterion function is compared with a threshold and results in the indicator function $I(t)$, which is 0 at points where the criterion function is less than the threshold and is 1 otherwise. The average value of the indicator function is the intermittency factor. The indicator function is used to mask parts of the data when the conditional statistics are being calculated (ref. 33).

In summary, the construction of the indicator function requires choosing a discriminator signal, a level of differentiation, a smoothing scale, and a threshold. A good algorithm is characterized by the results being insensitive to these choices and by the more subjective visual agreement between the indicator function and the traces of the raw data. The systematic testing reported in reference 32 supported the aforementioned recommendations. The present study used second derivatives of the streamwise velocity to construct the detector function. Smooth-

ing and thresholding were complicated by the absence of the reference values of a Taylor microscale and a corresponding velocity scale in the rapidly evolving spots. The recommendations of Sohn and Reshotko (ref. 5) were followed, and a smoothing scale of the order of 15 time steps was used, which verified that the results were insensitive to the particular value. For thresholding, a clean separation of the detector function into large and small values made very effective a threshold of the order of 1 standard deviation of the criterion signal. Again, the results showed little sensitivity to the selected value.

The indicator function $I(t)$ was then used to mask the energy map in the construction of the mean spectra. Analytically, the time integration in equation (7) is restricted to those portions of the signal where the indicator function is nonzero:

$$E_I(\kappa) = \frac{1}{2\pi} \int_{-\infty}^{\infty} \left| f_g(\kappa, t) \right|^2 I(t) \, \mathrm{d}t \tag{10}$$

This ability to select portions of the energy map to construct conditional spectra gives wavelet methods a flexibility that Fourier techniques do not have, as seen in references 16, 23, and 31 where it was used with different conditioning functions.

The conditional (turbulent) power spectrum $E_I(\kappa)$ and the corresponding energy content $\kappa E_I(\kappa)$ are compared with the ensemble means in figures 7 and 8. Figure 7 shows that turbulence conditioning captured virtually all the small-scale power density (durations shorter than 0.3 ms or frequencies larger than 0.84 kHz) so that the curves nearly coincide. This is not surprising because the intermittency criterion specifically screens for such fluctuations. In the energy-containing range (around 1.26 ms or 0.2 kHz), the turbulent intervals capture about 20 percent of the energy. If the energy were homogeneously distributed among the turbulent spots and the laminar regions, this value would be in proportion to the intermittency factor, calculated as 8 percent. The fact that a spot is associated with large-scale fluctuations more vigorous than those in the nonturbulent part was noted in relation to the velocity deficit associated with the spot at the end of the Wavelet Transforms section. The power spectra confirm the statistical validity of the observation.

The conditional energy content is shown in figure 8. A sharp drop in emphasis is seen in the range of 1.26 ms (0.2 kHz) and slight activity around 0.085 ms (3 kHz). A sharp increase in emphasis seen around 0.0252 ms (10 kHz) is attributed to aliasing noise. The conclusion is that no dominant scales are associated with the turbulent spot energy. The nearly uniform energy content indicates that the conditional power spectrum (fig. 7) has an extended range of 0.85 to 0.03 ms (0.3 to 8 kHz) with an approximate slope of κ^{-1}, which appears as a nearly constant value in the plot of $\kappa E(\kappa)$ in figure 8. The same conclusion was reached with quadrant conditioning of the power spectra (see the section Quadrant Maps, Histograms, and Conditional Spectra).

In summary, this section focused on energy considerations available from single signals. The advantage of time-frequency resolutions, displayed graphically by the energy maps, provides greater flexibility than that offered by similar Fourier methods, particularly in terms of conditional sampling. However, it was expected that turbulent spots would be particularly active and would yield dominant internal scales relevant to the parameterization of turbulent transport. The conclusion reached in the present study is that either the internal structure of the spots is comparatively inactive at this location, or that the techniques presented in this section failed to identify them. The next section will provide a definitive answer.

Focus on Momentum Transport

In this section, the emphasis shifts from the energy of a single signal to the Reynolds stress τ_R

$$\tau_R = -\rho \overline{uv} \tag{11}$$

which is obtainable from pairs of signals u and v and where ρ is the density.

Quadrant Maps, Histograms, and Conditional Spectra

One of the methods of isolating the Reynolds-stress-producing events in boundary layers is the quadrant-splitting method from reference 35. Streamwise and transverse velocity fluctuations can be positive or negative, dividing the u-v plane into four quadrants. The first quadrant is identified by a positive u (fluid faster than average) and positive v (fluid moving away from the wall). Counter clockwise from the first quadrant, the second quadrant is associated with slower fluid moving away from the wall (ejection), the third, with slower fluid moving toward the wall, and the fourth, with fast fluid coming toward the wall (sweep). In terms of the magnitude rather than the intermittency factor, the dominance of second- and fourth-quadrant events results in a positive Reynolds stress.

A variant of the quadrant-splitting method is scale-dependent quadrant splitting that is made possible by the scale resolution displayed in the wavelet map of figure 2. A quadrant indicator map can be constructed by scanning quadrant indicator tests at all successive durations. However, the interpretation of the result obtained by that method is difficult because the wavelet coefficients are not the local contributions to the signal. The inverse transform formula (ref. 2),

$$u(t) = \int_0^{\infty} \kappa^{1/2} \int_{-\infty}^{\infty} g_n\left[\kappa(t-\tau)\right] u_n(\kappa, \tau) \, \mathrm{d}\tau \, \mathrm{d}\kappa \tag{12}$$

shows that the local value of a signal includes wavelet coefficients from all nearby times, a convolution with the wavelet

similar to the transform formula (eq. (3)). Equation (12) is greatly simplified in the case of even-indexed Gaussian wavelets (ref. 30) for which

$$u(t) = \frac{(-1)^n \pi^{-1/2} 2^{-n+1/4}}{\Gamma(n)} \int_0^\infty \kappa^{-1/2} u_{2n}\left(\frac{\kappa}{\sqrt{2}}, t\right) \mathrm{d}\kappa$$

$$= \int_0^\infty U_n(\kappa, t)\, \mathrm{d}\kappa \tag{13}$$

Accordingly, the amplitude of the signal $u(t)$ can be reconstructed by a summation of the amplitude transform $U_n(\kappa,t)$ at instant t (rather than by a convolution involving neighboring times). Note that U_1 corresponds to the Mexican hat transform g_2, which is used in all the results presented.

The amplitude transform maps lend themselves to scale-dependent quadrant splitting. At each time and duration, a quadrant is identified from the signs of the amplitude transforms of the u- and v-signals. Figure 9 shows the result and a v-trace from which the spot can be identified easily. The plots map the islands of quadrant identification (value 1) over the reference value 0 in the time-duration domain. In the second quadrant, note that the long-duration ejections extending over at least a decade from 0.6 ms and larger (0.42 kHz and lower frequencies) seem to be associated with turbulent spots, an observation that will be confirmed in the next section. The observation that certain ranges of durations appear more crowded in some quadrants (e.g., that the third quadrant contains more events in the 1.0-ms (0.25-kHz) range than does the second or fourth) is not supported by the calculation of the intermittency factor as a function of duration in each quadrant (plotted in fig. 10). Except for the noise-related increase in intermittency in the first and third quadrants (same-sign fluctuations of u and v) at very short durations, the intermittency factors do not depart much from the equidistribution value of 25 percent. Minor differences of the order of 5 percent can be observed in the range of 0.1 to 3 ms (2.5 to 0.084 kHz) with the larger values occurring in the second and fourth quadrants. This equidistribution among the scale-dependent quadrants contrasts with the quadrant intermittency factors based on the raw signals for which the intermittency factors are calculated to be 0.34, 0.16, 0.20 and 0.30 for quadrants 1 to 4, respectively.

In the section Conditional Stress Maps, it will be shown that this nearly uniform distribution of intermittency factors between quadrants is not reflected by the corresponding stress distribution. The magnitude of the contributions to the stress will be the subject of the following subsections.

Correlation Maps

It is well known (ref. 36) that in turbulent flows, correlations between velocity components or between velocity and scalar fields such as temperature indicate the presence of turbulent fluxes of momentum or concentration. These terms are important to the flow dynamics, and their modeling relies extensively on the adequate characterization of the length and time scales associated with the transport process.

The energy spectra provided one definition of dominant time scales, which have the advantages of being easy to compute and being available from single-wire data (as in ref. 16). However, the failure of the time scales to identify a significant role of the turbulent spots in figure 8 provides motivation to identify alternatives. This section uses one of the most innovative and successful wavelet tools introduced in references 24 and 25.

Consider the Reynolds stress component $-\rho\overline{uv}$. By making use of the amplitude transform (eq. (13)), it can be rewritten in the form

$$\tau_R = -\rho\overline{uv} = -\rho \frac{1}{T} \int_0^T u(t)v(t)\, \mathrm{d}t$$

$$= -\rho \frac{1}{T} \int_0^T \int_0^\infty U_n(\kappa_u, t)\, \mathrm{d}\kappa_u \int_0^\infty V_n(\kappa_v, t)\, \mathrm{d}\kappa_v\, \mathrm{d}t$$

$$= -\rho \int_0^\infty \int_0^\infty \overline{U_n(\kappa_u, t) V_n(\kappa_v, t)}\, \mathrm{d}\kappa_u\, \mathrm{d}\kappa_v$$

$$= -\rho \int_{-\infty}^\infty \int_{-\infty}^\infty \kappa_u \kappa_v \overline{U_n(\kappa_u, t) V_n(\kappa_v, t)} \cdot \mathrm{d}(\log \kappa_u)\, \mathrm{d}(\log \kappa_v) \tag{14}$$

Therefore, the Reynolds stress can be decomposed into contributions from the plane of the logarithm of the durations of each component signal. As in the case of the power spectrum, multiplying by the corresponding inverse durations yields a quantity that is proportional to the transport accomplished within a pair of scale ranges. The expression $-\rho\kappa_u\kappa_v\overline{U_n V_n}$ is called the spectral Reynolds stress content (for short, Reynolds stress map).

In the Reynolds stress map of figure 11, the axes are logarithmic and span the durations of u (abscissa) and v (ordinate). The color contour lines represent lines of constant Reynolds stress density as color coded in the scale. If one thinks of the Reynolds stress map as a surface, the volume under that surface is equal to the Reynolds stress. The diagonal structure of this map is notable because it expresses quantita-

tively the commonly held belief that velocity components can be well correlated only if they are in the same range of time scales (or frequencies). Figure 11 shows several groups of dominant active scales separated by factors of the order of 4 to 5. Because modeling has to capture the correct physics, this separation of active scales should be reflected in the model as discussed in the Conclusions.

The contrast between the dominant scales identified from energy considerations (fig. 6) and from momentum transport (fig. 11) is striking. The unique energy peak at a wavelet duration of about 1.25 ms (corresponding to 0.2 kHz) is divided into two active scales on the Reynolds stress map: one at 2.5 ms (0.1 kHz and labeled A) and one at about 0.6 ms (0.42 kHz and labeled B). These scales are associated with the nonturbulent part of the signal. The frequency ratio of 4 between these nonturbulent scales is unexplained. Note that none of these scales is in the correct range (0.28 ms or 0.9 kHz) to be associated with Tollmien-Schlichting waves. Furthermore, the frequency range typical of turbulent spots and conspicuously missing from figure 6 is clearly visible in the 0.05-ms (5-kHz) range on the Reynolds stress map (labeled C). The combination of low energy content and large contribution to transport led to the hypothesis that the turbulent spot fluctuations are highly correlated (addressed in the next section). Finally, note that the dark circular area in the upper right corner of figure 11 is associated with aliasing noise.

Spectral Correlation Coefficients

This section focuses on the correlation coefficients for the spectral contributions to u and v. The correlation coefficients are derived by normalizing $\overline{U_n(\kappa_u,t)V_n(\kappa_v,t)}$ by the respective standard deviations U_n' and V_n' of $U_n(\kappa_u,t)$ and $V_n(\kappa_v,t)$, respectively. Recall that wavelet transforms have a zero mean as a result of the admissibility condition (ref. 2). Thus,

$$U_n' = \sqrt{\overline{U_n^2}} \tag{15}$$

Then the spectral correlation map is simply the plot of

$$\kappa_u\kappa_v \frac{\overline{U_n(\kappa_u,t)V_n(\kappa_v,t)}}{U_n'V_n'} \tag{16}$$

as a function of κ_u and κ_v and is shown in figure 12. The large-scale transport is associated with correlation coefficients of the order of –0.3 (2.5 ms or 0.1 kHz) and –0.2 (0.6 ms or 0.42 kHz). At the shorter durations associated with the turbulent spots (fig. 13), the correlation coefficients are much larger, reaching –0.45. This high level of correlation is indicative of very strong interactions that organize the velocity field. Although the energy content of these fluctuations is relatively low, the combination with high levels of correlation yields one of the dominant contributions to the transport of momentum (fig. 11).

Conditional Stress Maps

Stress maps similar to that shown in figure 11 can be constructed by masking out unwanted parts of the data to calculate conditional stress maps. This selective process was implemented with the maps in the section Energy Maps and will now be used to focus on the different classes of events and their contributions to the momentum transport. Four types of conditioning criteria have been considered:

(1) Laminar-turbulent
(2) Quadrant
(3) Scale-dependent quadrant
(4) Event-based (local maxima of energy, as in ref. 23).

In the case of event-based conditioning (4), the results were rather uninteresting, which indicated a poor match between energetic fluctuations and momentum transport. The results obtained from the first three types of criteria are presented in the following sections.

Laminar-turbulent conditional scales of momentum transport.—The conditional Reynolds stress maps are built from sampling portions of the signals that are simultaneous with the presence or absence of turbulent spots, as indicated by the function $I(t)$ in

$$-\rho\overline{uv}_I = -\rho\int_{-\infty}^{\infty}\int_{-\infty}^{\infty}\kappa_u\kappa_v\overline{U_n(\kappa_u,t)V_n(\kappa_v,t)I(t)}\cdot \mathrm{d}(\log\kappa_u)\,\mathrm{d}(\log\kappa_v) \tag{17}$$

and the result is shown in figure 13. The figure shows that the large-scale transport islands (2.5 and 0.6 ms or 0.1 and 0.42 kHz, labeled A and B) appear only in the laminar-conditioned map, whereas the small-scale island (labeled C) appears only in the turbulent-conditioned map. The isolation of the large-scale transport islands to be mutually exclusive with the presence of spots is striking in view of the considerable energy content of the spots (as shown in fig. 7) in this range of durations. This implies that only a fraction of the energetic fluctuations is active in momentum transport, and this only between spots. This idea is developed further in the next section.

The laminar-conditioned stress map also shows two peaks of positive u-v at the off-diagonal locations (labeled D and E), indicating interactions between the two largest active scales. The reason these peaks do not appear on the ensemble stress map (fig. 11) is that it is not simply the sum of the two complementary conditional maps. This is easily seen from the following relations in which u and v stand for the instantaneous velocities rather than for the fluctuations:

$$\overline{(u-U)(v-V)} = \overline{(u-U)(v-V)I} + \overline{(u-U)(v-V)(1-I)}$$

$$= \overline{(u-U_I)(v-V_I)I} + \overline{(u-U_{1-I})(v-V_{1-I})(1-I)}$$

$$+ \bar{I}\,\overline{(1-I)}(U_I - U_{1-I})(V_I - V_{1-I})$$

$$= \overline{uv}_I + \overline{uv}_{1-I} + \bar{I}\,\overline{(1-I)}(U_I - U_{1-I})(V_I - V_{1-I}) \qquad (18)$$

In this relation, $U_I = \overline{UI}/\bar{I}$ is the conditional mean estimated over the turbulent portion of the signal. From equation (18), note that the ensemble stress map results from the addition of the turbulent- and laminar-conditioned stress maps and an extra term dependent on the differences between the conditional means and the intermittency factor $\bar{I}$.

Quadrant-conditioned stress maps.—According to this conditioning criterion, the only contributions sampled are those associated with the quadrant decomposition of the velocity signals (i.e., conditioning with the quadrant indicator function). The results are presented in figure 14 where the magnitudes of Reynolds stress densities are plotted on the same scale to facilitate comparisons. The figure shows that quadrants 1 and 4 are practically inactive in the transport of momentum, with all dominant contributions taking place in quadrants 2 and 3, that is, with the streamwise velocity below average values. These two quadrants show a combination of symmetry and antisymmetry. Along the diagonal, all contributions are negative (wallward transport), with the second quadrant dominating. The off-diagonal components indicate the coexistence of long-duration streamwise fluctuations u (abscissa) with short-duration transverse fluctuations v (ordinate). The correlation is negative in quadrant 2 and positive in quadrant 3. Therefore, it appears as though, over a range of durations of a decade and a half, the sign of long-duration transverse velocity fluctuations responsible for the quadrant labeling applies on average to shorter durations as well. These observations contrast the near uniformity in intermittency factors discussed in the Quadrant Maps section.

Spectral-quadrant-conditioned stress maps.—A variant of quadrant conditioning is sampling points in the time-duration plane of each amplitude transform map so that the corresponding spectral contribution to the u- and v-signals is in the same quadrant. This is accomplished by masking both u- and v-maps with the same spectral quadrant indicator map shown in figure 9. The results are displayed in figure 15. These subsets of the original data show that most of the stress is associated with the turbulent spots in quadrants 2 and 4; shorter duration laminar contributions (0.6-ms or 0.42-kHz range) have opposite signs. Off-diagonal components in quadrants 2 and 3 show that a negative u is weakly correlated with v-fluctuations of either sign at equal or longer durations.

Intermittency of Reynolds-Stress-Producing Events

From the previous sections and figures 11 to 15, spectral contributions to the Reynolds stress were identified. The various plots reveal an overall consistency, particularly for the contributions from the turbulent spots on the upper right portion of the diagonals and a puzzling scatter of active islands on and off the diagonal, particularly in the lower left corner of the plots. The need to understand the significance of these islands led to a study of the history of the associated correlations, and the result is shown in figure 16.

Three representative durations close to the peaks of the stress map were chosen: 2.24, 1.2, and 0.08 ms (0.11, 0.21, and 3.1 kHz). These durations were plotted in figure 16 with the matching histories of (1) the turbulence indicator function (spot identifier); (2) the instantaneous contribution to the energy; (3) the instantaneous contribution to the Reynolds stress; and (4) the instantaneous contribution to the energy flux (see the next section). The figure presents the entire length of the available records, which makes plotting the velocity traces impractical in this instance. The indicator function is shown instead, highlighting the locations of the spots. Values were normalized to unit variance (except for the indicator functions); then values in excess of three standard deviations were truncated to provide an adequate depiction of the smaller values, eliminating from the plots the clutter of large spikes. Also plotted (dashed lines) were the cumulative energy, stress, and energy flux so that the contributions from very large events could be measured according to their relative contributions (the cumulative curves are normalized by their extreme value).

In figure 16 (a) at the longer duration of 2.24 ms (0.11 kHz), the energy is only loosely associated with the presence of spots. The nonnegative values of instantaneous energy build up the cumulative value gradually, with an occasional small jump such as that seen at a time of 300 ms. This relatively smooth evolution contrasts with that of the Reynolds stress curve for which energetic packets (e.g., at 150 and 200 ms) do not always contribute to the cumulative stress (or contribute negatively) and the largest part of the cumulative spectral stress is accounted for by individual jumps. The number of these events at large duration scales is too small to produce convergent statistics with the present signal length and therefore are called rare events. This observation may explain the "lumpy" appearance of some of the stress maps and conditional stress maps at the longer duration ranges in that a few large events are likely to determine the magnitude of the cumulative value. An example of a dominant rare contributor can be seen in figure 16(b) at a time of 350 ms. The gradual Reynolds stress buildup leading to this (spot-related) event would be canceled by the subsequent decrease in cumulative stress.

At shorter durations (0.08 ms or 3.1 kHz) typical of spot-generated turbulence shown in figure 16(c), the spots themselves become typical contributors, as would be expected, but the larger number of them available in our records leads to a smoother and more nearly monotonous buildup of the cumulative spectral stress. Departures from the linear growth of the cumulative energy and Reynolds stress are smaller, indicating that individual events have less impact on the cumulative value than they have at longer durations.

Higher Order Correlations

The correlation methods presented in the previous section can be applied to higher order moments. For example, the kinetic energy fluxes can be mapped by correlating an energy map (u^2 in this section) with the amplitude wavelet map of another velocity component (v in this instance). The interpretation (fig. 3) of $\int_0^\infty d\kappa \left| u_g(\kappa,t) \right|^2 / 2\pi$ as instantaneous energy can be used to estimate the spectral content energy fluxes of the type $\overline{u^2 v}$. Then,

$$\overline{u(t)^2 v(t)} \sim \frac{1}{2\pi} \int_0^\infty d\kappa_u \int_0^\infty \overline{\left| u_2\left(\kappa_{u^2}, t\right) \right|^2 V_1\left(\kappa_v, t\right)} \cdot d\kappa_v$$

$$= \frac{1}{2\pi} \int_{-\infty}^\infty d(\log \kappa_u) \int_{-\infty}^\infty \kappa_u \kappa_v \overline{\left| u_2\left(\kappa_{u^2}, t\right) \right|^2 V_1\left(\kappa_v, t\right)} \cdot d(\log \kappa_v) \tag{19}$$

Figures 17 to 20 show the spectral energy flux content measured by the integrand in equation (19). The ensemble flux map in figure 17 is remarkable for several features. First, there is a positive correlation between excess energy and motion away from the wall for all pairs of durations. Second, the upper diagonal structure of the map shows that energy fluctuations at one given duration seem correlated with a positive v at all durations comparable or smaller. In particular, a vertical band on the left side of the plot shows that energy in the 2.5-ms (0.1-kHz) range is correlated with normal velocities at all durations, and the horizontal band in the middle of the plot shows that transverse velocities in the 0.15-ms (1.7-kHz) range are strongly correlated with energy fluctuations at the larger durations. This may indicate a coupling between the activity of the spot in the 0.1-ms (2.5-kHz) range and the energy fluctuations in the 2.5-ms (0.1-kHz) range. Finally, the lumpiness of the map seems to indicate active frequency bands: 0.8 and 2.5 ms (0.31 and 0.1 kHz) of u^2 with 1 ms (0.25 kHz) of v, 2.5 and 0.1 ms (0.1 and 2.5 kHz) of u^2 with 0.15 ms (1.7 kHz) of v, and finally 0.08 ms (3.1 kHz) of u^2 with 0.06 ms (4.2 kHz) of v in addition to short-duration noise.

When the flux map is conditioned by sampling only turbulent or laminar portions of the signals, the result is shown in figure 18. For turbulent conditioning, the map is approximately diagonal, with three of the islands identified above dominating the energy flux. The laminar statistics are predominantly at 0.5 ms (0.5 kHz) of u^2 and 1.0 ms (0.25 kHz) of v but are negative and have a magnitude comparable to that of the turbulent-conditioned fluxes. Hence, it may be concluded that all off-diagonal features of figure 17 can be attributed to differences in the conditional means of u^2 and v in the laminar and turbulent regions.

Figure 19 shows the quadrant distribution of the energy fluxes. Again, quadrants 1 and 4 are basically inactive whereas quadrants 2 and 3 (i.e., streamwise velocity smaller than average) have a lower diagonal structure. It is surmised that the off-diagonal contributions are again the result of different sample means.

The quadrant-conditioned correlation coefficients are reproduced in figure 20. A lumpy diagonal structure is visible in all quadrants, with large correlation coefficients in quadrant 2 and in the short durations characteristic of the spots. The lumpy structure of these maps is clearly due to the few rare events that account for a significant part of the cumulative value of $u^2 v$ at all durations, as seen in figures 16 (a) to (c). It is concluded that the flux maps presented here are mostly illustrative of the potential of the method but are based on records too short to ensure statistical convergence.

Conclusions

The conclusions are presented at four levels:

1. At a general level,

   (a) Experimental and numerical data contain much more information than that made available by conventional methods of signal analysis. In the wavelet representation, much of that information is made more accessible by the time-frequency resolution.

   (b) Our procedure consists of two major steps: mapping the data in the time-frequency domain and reducing the volume of information by statistical means. By using only the Mexican hat wavelet (a relatively simple wavelet), a large number of ensemble and conditional statistics have been devised. Many more can conceivably be explored, and other wavelets will emphasize other features in the data.

(c) As in the cited cases of other data explored by similar methods, new algorithms were tested in this project and provided answers to new questions. Selecting the more useful algorithms will remain a considerable task until experience reveals those that show the most promise.

(d) The new statistics calculated are quantitative and can be used to compare related data sets. With more diagnostic tools available, significant differences in the underlying physics are more likely to be exposed.

2. With regard to the specific flow physics of this data set,

(a) The dynamical role played by the internal structure of the spots is highlighted differently by energy-related and Reynolds-stress-related methods. Free-stream turbulence and spot-related fluctuations in the nonturbulent portions of the flow (between spots) are energetically dominant whereas the fluctuations internal to the spots are much less energetic but dominate the momentum transport.

(b) This conclusion has major implications for data collection and filtering in transitional flows because transport is at the core of all modeling efforts. Preservation of the energetic events cannot be viewed as a satisfactory criterion.

(c) Contributions to the momentum transport were much more intermittent than the contributions to the fluctuating energy. At the smaller time scales, a large collection of events is nonetheless obtained, and statistics can be considered stable. However, at the longer time scales, the rare major events included in the records dominate the magnitude and time-scale of the statistics.

(d) The use of longer records, or a large number of smaller independent samples, is required to yield stable statistics of the shear stress and the higher moments. This has been known for a long time, but the rates of convergence are likely to be much slower with rare events than they would be with a stationary signal.

3. With respect to the reduction of the data and the extraction of time scales,

(a) The ultimate reduction of the data consists of the extraction of a few simple parameters. In the case of the pair of anemometry signals examined in this report, the focus was deliberately on the extraction of meaningful time scales from the data. The reason is that once dominant energy and time scales are defined and quantified, they can be used for engineering modeling. The modeling of boundary layer transition in noisy and/or transient industrial flows could benefit from a systematic documentation of eddy viscosities by these methods.

(b) The time scales are constructed in various ways by sorting the information according to scale using wavelet transforms. In contrast to Fourier-based spectral discrimination, it was possible to identify individual events, screen them according to various criteria, and construct meaningful time scales attached to different classes of events.

(c) The contrast in the time scales obtained from single-signal, energy-based statistics and two-signal, stress-based statistics is relevant not only to the physical understanding of transitional flows but also to the modeling of these flows.

4. With regard to future work,

(a) The techniques presented here provide the basis for abundant future work that will be pursued in several directions. The spatial evolution of the statistics developed here is reported in a separate paper. Spectral information about the internal structure of spots may result in a better understanding of receptivity, formation, and evolution.

(b) The application of other wavelets may enhance different features in the signals and yield valuable statistics to complement the current results.

(c) Finally, other statistical quantities such as scale-dependent probability distributions and moments are being developed.

In conclusion, wavelet tools were used to gain insight into the physics and dynamics of the flow. The full impact of this work will be seen in the potential future use of these results for engineering modeling. Scale-dependent physics, particularly scale-dependent dynamics and transport, must be incorporated in the models if great improvements in them are to be realized.

Lewis Research Center
National Aeronautics and Space Administration
Cleveland, Ohio, July, 1997

References

1. Bendat, J.S.; and Piersol, A.G.: Random Data: Analysis and Measurement Procedures. John Wiley & Sons, New York, 1986.
2. Daubechies, I.: Ten Lectures on Wavelets. Society for Industrial and Applied Mathematics, Philadelphia, PA, 1992.
3. Farge, M.: Wavelet Transforms and Their Applications To Turbulence. Ann. Rev. Fluid Mech. vol. 24, 1992, pp. 395–457.
4. Meyer, Y.: Wavelets: Algorithms and Applications. Society for Industrial and Applied Mathematics, Philadelphia, PA, 1993.
5. Sohn, K.H.; and Reshotko, E.: Experimental Study of Boundary Layer Transition With Elevated FreestreamTurbulence on a Heated Flat Plate. NASA CR–187068, 1991.
6. Sohn, K.H.; Zaman, K.B.M.Q.; and Reshotko, E.: Turbulent Heat Flux Measurements in a Transitional Boundary Layer. NASA TM–105623, 1992.
7. Klebanoff, P.S.; Tidstrom, K.D.; and Sargent, L.M.: The Three-Dimensional Nature of Boundary Layer Instability. J. Fluid Mech. vol. 12, 1962, pp. 1–34.
8. Nishioka, M.; and Morkovin, M.V.: Boundary Layer Receptivity to Unsteady Pressure Gradients, Experiments, and Overview. J. Fluid Mech., vol. 171, Oct. 1986, pp. 219–261.
9. Breuer, K.S.; and Landahl, M.T.: The Evolution of a Localized Disturbance in a Laminar Boundary Layer. Part II—Strong Disturbances. J. Fluid Mech., vol. 220, Nov. 1990, pp. 595–621.
10. Govindarajan, R.; and Narasimha, R.: The role of Residual Non-Turbulent Disturbances on Transition Onset in Two-Dimensional Boundary Layers. J. Fluid Eng. Trans. ASME, vol. 113, Mar. 1991, pp. 147–149.
11. Kim, J.; Simon, T.W.; and Russ, S.G.: Free-Stream Turbulence and Concave Curvature Effects on Heated, Transitional Boundary Layers. J. Heat Transfer Trans. ASME, vol. 114, May 1992, pp. 338–347.
12. Morkovin, M.V.: Bypass Transition Research: Issues and Philosophy. in Instabilities and Turbulence in Engineering Flows. D.E. Ashpis, T.B. Gatski, and R. Hirsh, eds., Kluwer Academic Publishers, Dordrecht, Netherlands, 1993, pp. 3–30.
13. Wang, T.: An Experimental Investigation of Curvature and Freestream Turbulence Effects on Heat Transfer and Fluid Mechanics in Transitional Boundary Layers. Ph.D. Thesis, Univ. of Minnesota, 1984.
14. You, S.M.; Kim, J.; and Simon, T.W.: Free-Stream Turbulence Effects on Convex-Curved Turbulent Boundary Layers. J. Heat Transfer, Trans. ASME, vol. 111, Feb. 1989, pp. 66–72.
15. Schobeiri, M.T.; and Radke, R.E.: Effects of Periodic Unsteady Wake Flow and Pressure Gradient on Boundary Layer Transition along the Concave Surface of a Curved Plate. ASME Paper 94–GT–327, 1994.
16. Schobeiri, M.T.; Read, K.; and Lewalle, J.: Effect of Unsteady Wake Passing Frequency on Boundary Layer Transition, Experimental Investigation and Wavelet Analysis. ASME Paper 95–GT–437, 1995.
17. Simon, F.: The Use of Transition Region Characteristics to Improve the Numerical Simulation of Heat Transfer in Bypass Transitional Flows. NASA TM–106445, 1993.
18. Simon, F.F.; and Stephens, C.A.: Modeling the Heat Transfer in Bypass-Transitional Boundary Layer Flows. NASA TP–3170, 1991.
19. Simoneau, R.J.; and Simon, F.F.: Progress Toward Understanding and Predicting Heat Transfer in the Turbine Gas Path. Int. J. Heat and Fluid Flow, vol. 14, no. 2, June 1993, pp. 106–128.
20. LaGraff, J.E.; Ashworth, D.A.; and Schultz, D.L.: Measurement and Modeling of the Gas Turbine Blade Transition Process as Disturbed by Wakes. J. Turbomachinery, vol. 111, July 1989, pp. 315–322.
21. Mayle, R.E.: The Role of Laminar-Turbulent Transition in Gas Turbine Engines. ASME Report 91–GT–261, 1991.
22. Dallard, T.; and Browand, F.K.: The Growth of Large Scales at Defect Sites in the Plane Mixing Layer. J. Fluid Mech., vol. 247, Feb. 1993, pp. 339–368.
23. Higuchi, H.; Lewalle, J.; and Crane, P.: On the Structure of a Two-Dimensional Wake Behind a Pair of Flat Plates. Phys. Fluids, vol. 6, no. 1, Jan. 1994, pp. 297–305.
24. Lewalle, J.: Wavelet Analysis of Experimental Data: Some Methods and the Underlying Physics. AIAA Paper 94–2281, 1994.
25. Lewalle, J.; Petagna, P.; and Buresti, G.: Wavelet Statistics of the Near-Field Structure of a Coaxial Jet. AIAA Paper 94–2323, 1994.
26. Lewis, C.G.; and Gharib, M.: An Exploration of the Wake Discontinuity in Cylinder Diameter. Phys. Fluids A, vol. 4, Jan. 1992, pp. 104–117.
27. Spedding, G.R., et al.: A 2-D Complex Wavelet Analysis of an Unsteady Wind-Generated Surface-Wave Field. Dyn. Atmos. Oceans, vol. 20, nos. 1–2, Nov. 1993, pp. 55–78.
28. Brasseur, J.G.; and Wang, Q.: Structural Evolution of Intermittency and Anisotropy at Different Scales Analyzed Using Three-Dimensional Wavelet Transforms. Phys. Fluids A, vol. 4, no. 11, Nov 1992, pp. 2538–2554.
29. Meneveau, C.: Analysis of Turbulence in the Orthonormal Wavelet Representation. J. Fluid Mech., vol. 232, Nov. 1991, pp. 469–520.
30. Lewalle, J.: Wavelet Transforms of Some Equations of Fluid Mechanics. Acta Mech. vol. 104, 1994, pp. 1–25.
31. Lewalle, J.; Peek, F.W.; and Murphy, S.J.: Wavelet Analysis of the Olfactory Nerve Response to Stimulus. J. Theor. Biol. vol. 177, no. 3, Dec. 1995, pp. 215–236.
32. Hedley, T.B.; and Keffer, J.F.: Turbulent/Non-Turbulent Decisions in an Intermittent Flow. J. Fluid Mech., vol. 64, 1974, pp. 625–644.
33. Antonia, R.A.: Conditional Sampling in Turbulence Measurement. Annu. Rev. Fluid Mech., vol. 13, 1981, pp. 131–156.
34. Kuan, C.L.; and Wang, T.: Investigation of the Intermittent Behavior of Transitional Boundary Layers Using a Conditional Averaging Technique. Exp. Therm. Fluid Sci., vol. 3, Mar. 1990, pp. 157–173.
35. Wallace, J.M.; Ecklemann, H.; and Brodkey, R.S.: The Wall Region in Turbulent Shear Flows of Oil Investigated by Hot Film Measurement Technique and Anemometer Signal Analysis. J. Fluid Mech., vol. 54, June 1972, pp. 39–48.
36. Tennekes H.; and Lumley, J.L.: A First Course in Turbulence. M.I.T. Press, Cambridge, MA, 1972.

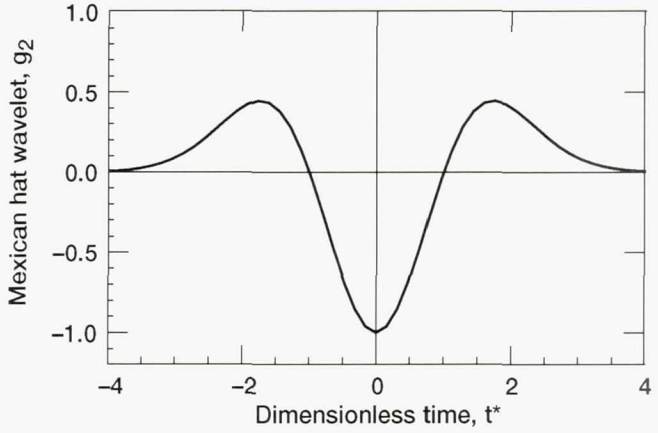

Figure 1.—Mexican hat wavelet, g_2.

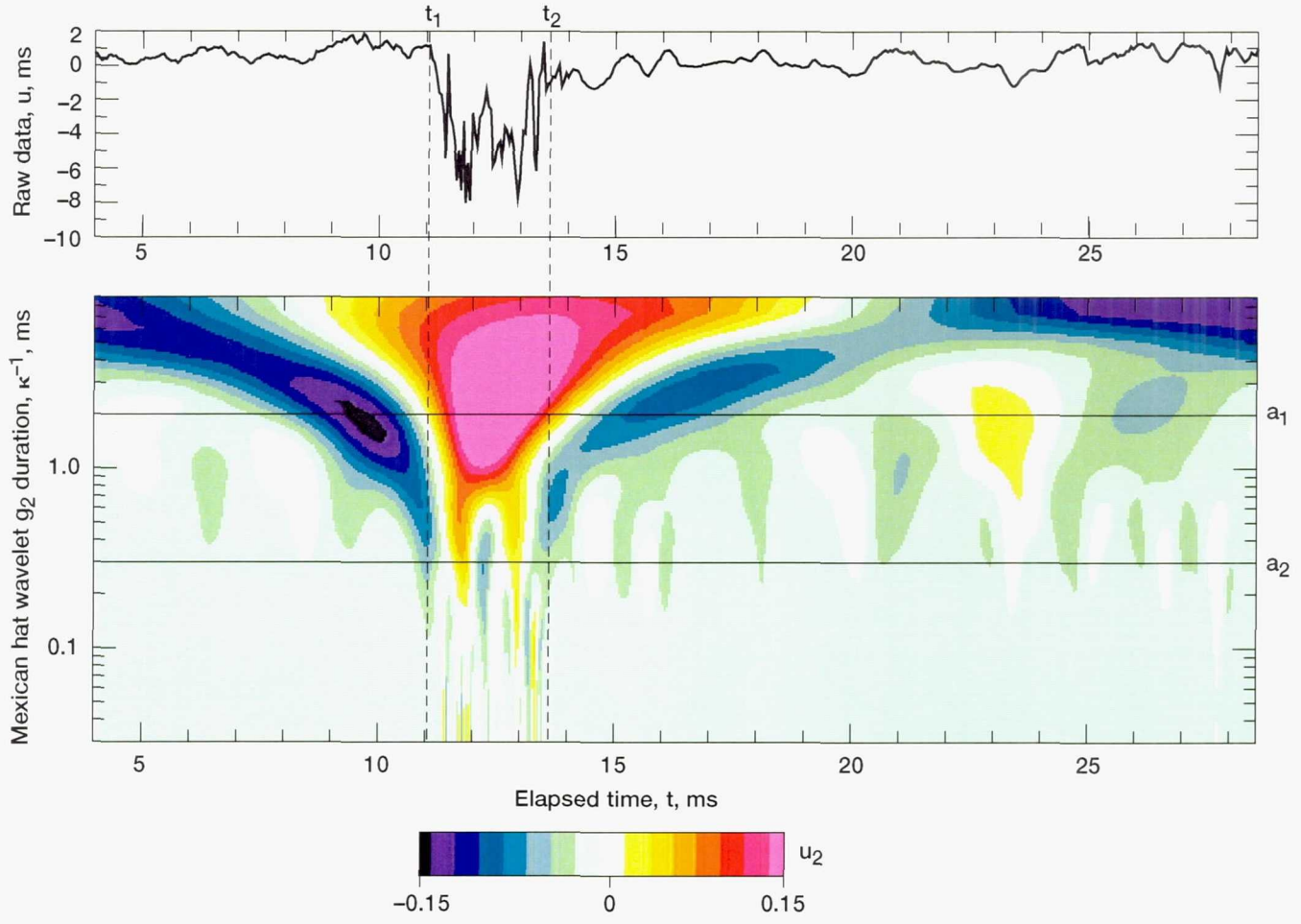

Figure 2.—Excerpt from streamwise velocity trace u(t) and its Mexican hat g_2 wavelet map $u_2(\kappa,t)$ in $ms^{-1/2}$.

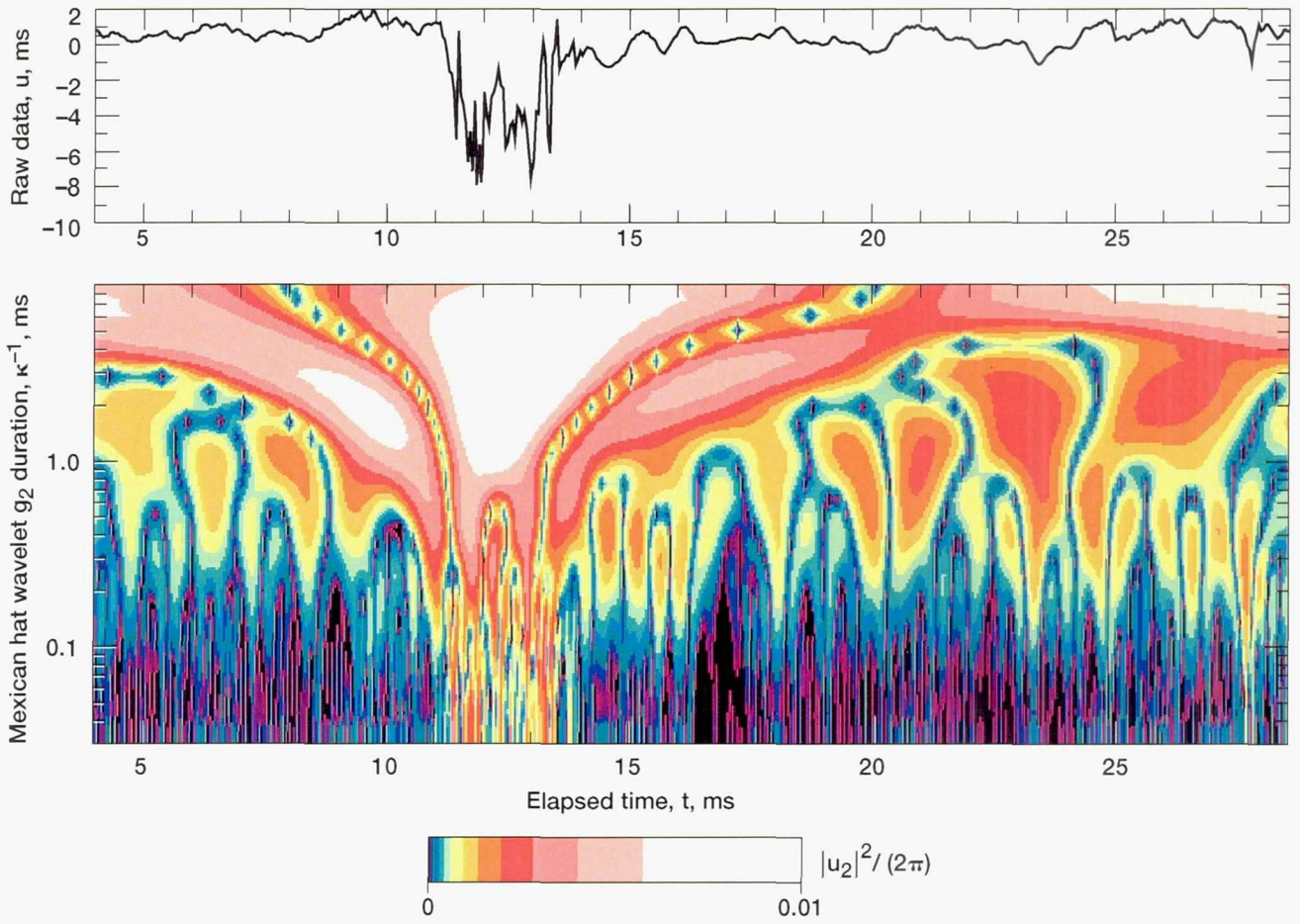

Figure 3.—Energy map $|u_2(\kappa,t)|^2/(2\pi)$ for streamwise velocity trace excerpt u(t) (same as fig. 2).

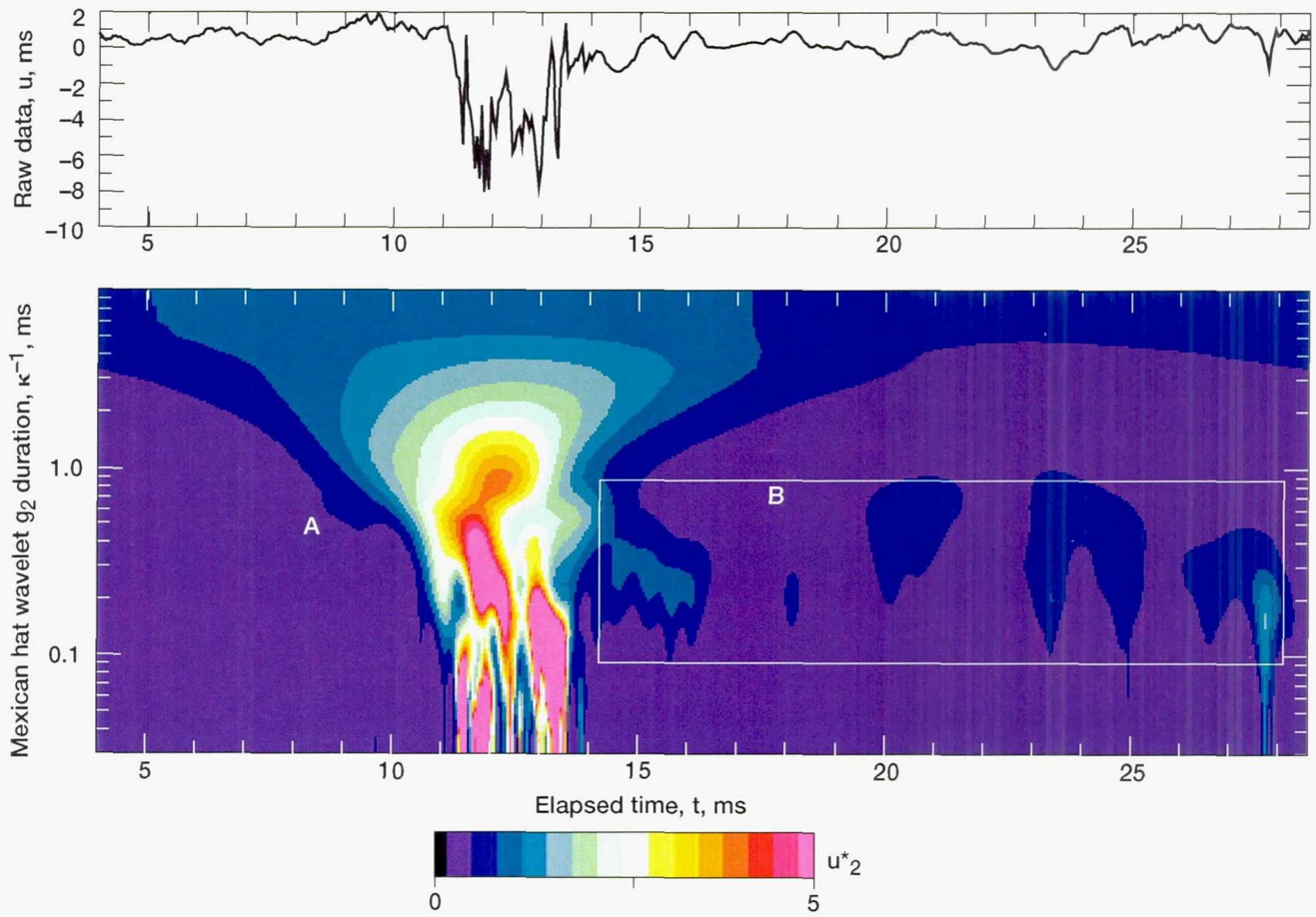

Figure 4.—Smoothed and normalized version of energy map of figure 3. Note hints of internal spot structure, which could be Tollmien-Schlichting packets.

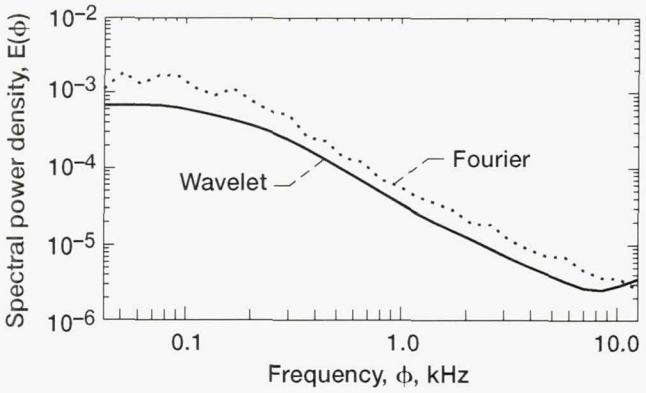

Figure 5.—Mean wavelet spectrum and Fourier power spectrum are generally featureless.

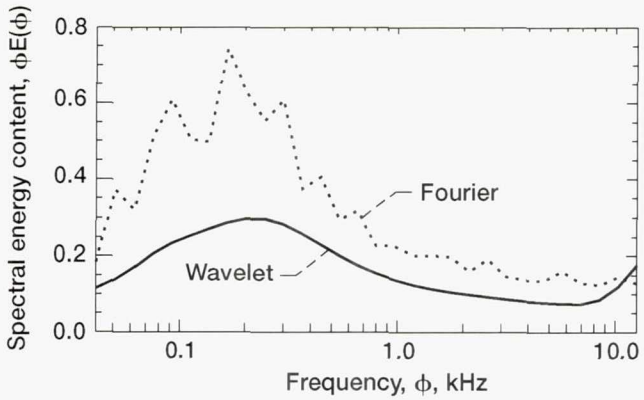

Figure 6.—Wavelet mean spectral energy content at various frequencies and Fourier counterpart. (Multiplying the power spectra in fig. 5 by the corresponding frequencies yields the wavelet mean spectral energy content.)

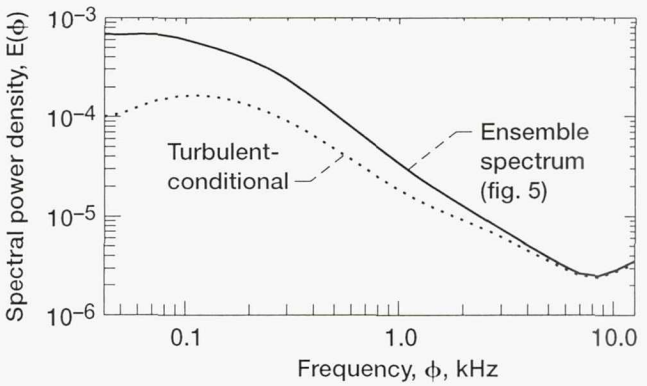

Figure 7.—Conditional wavelet spectrum obtained by including only contributions to the total energy that are simultaneous with the presence of small-scale turbulence.

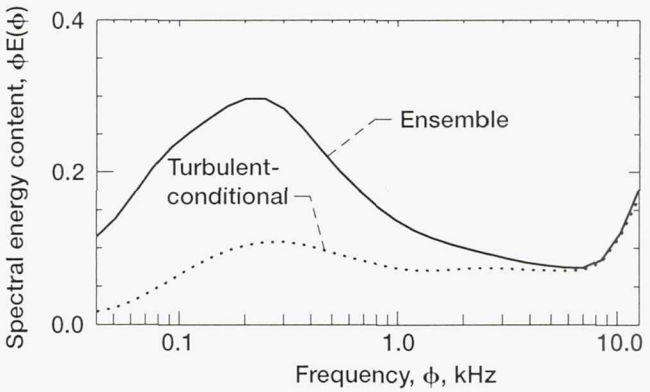

Figure 8.—Conditional energy content in turbulent spots (Except for noisy high-frequency fluctuations, no dominant scales are associated with turbulent spot energy.)

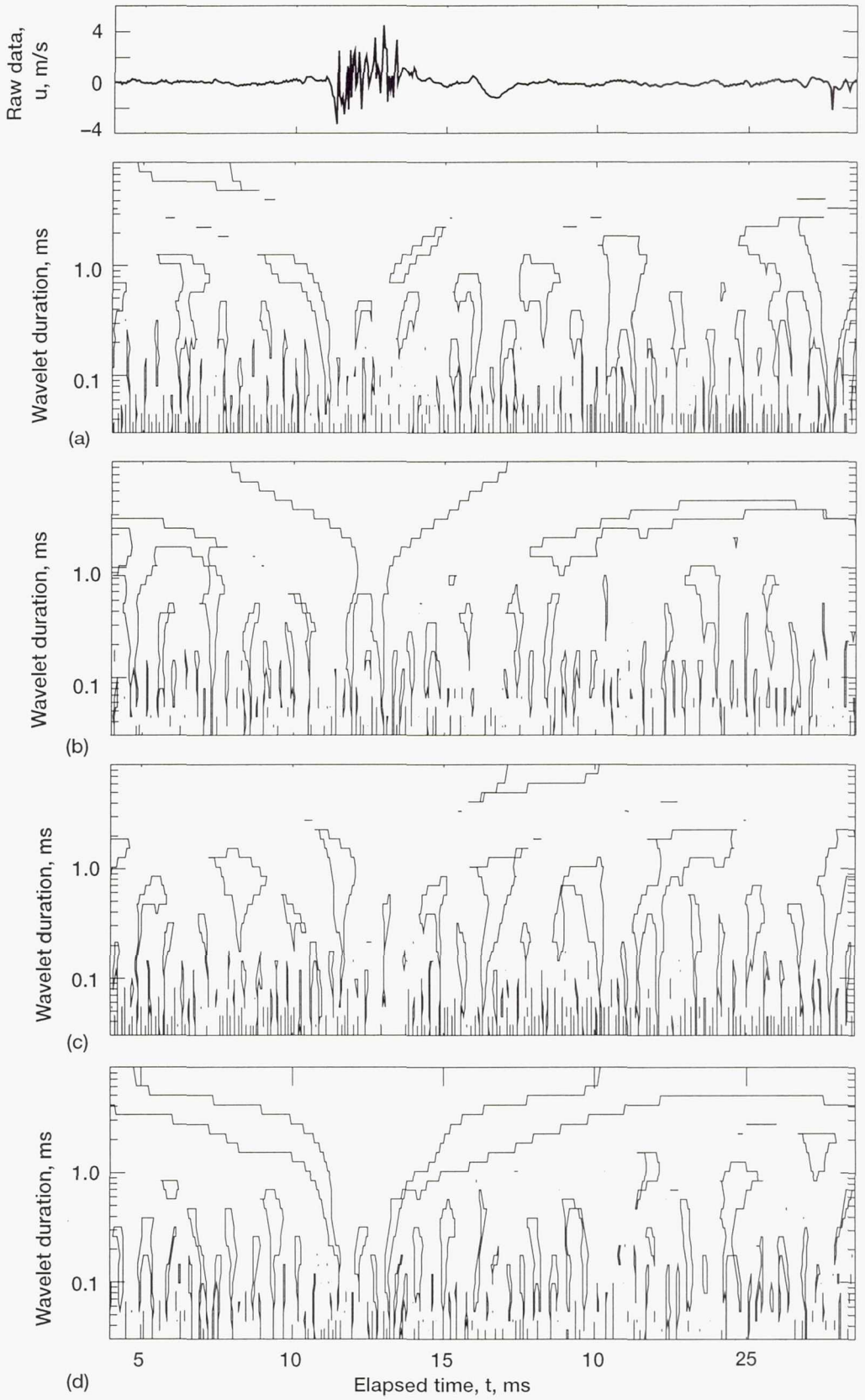

Figure 9.—Quadrant maps indicating that spots may be associated with large scale ejections. (a) Quadrant 1. (b) Quadrant 2. (c) Quadrant 3. (d) Quadrant 4.

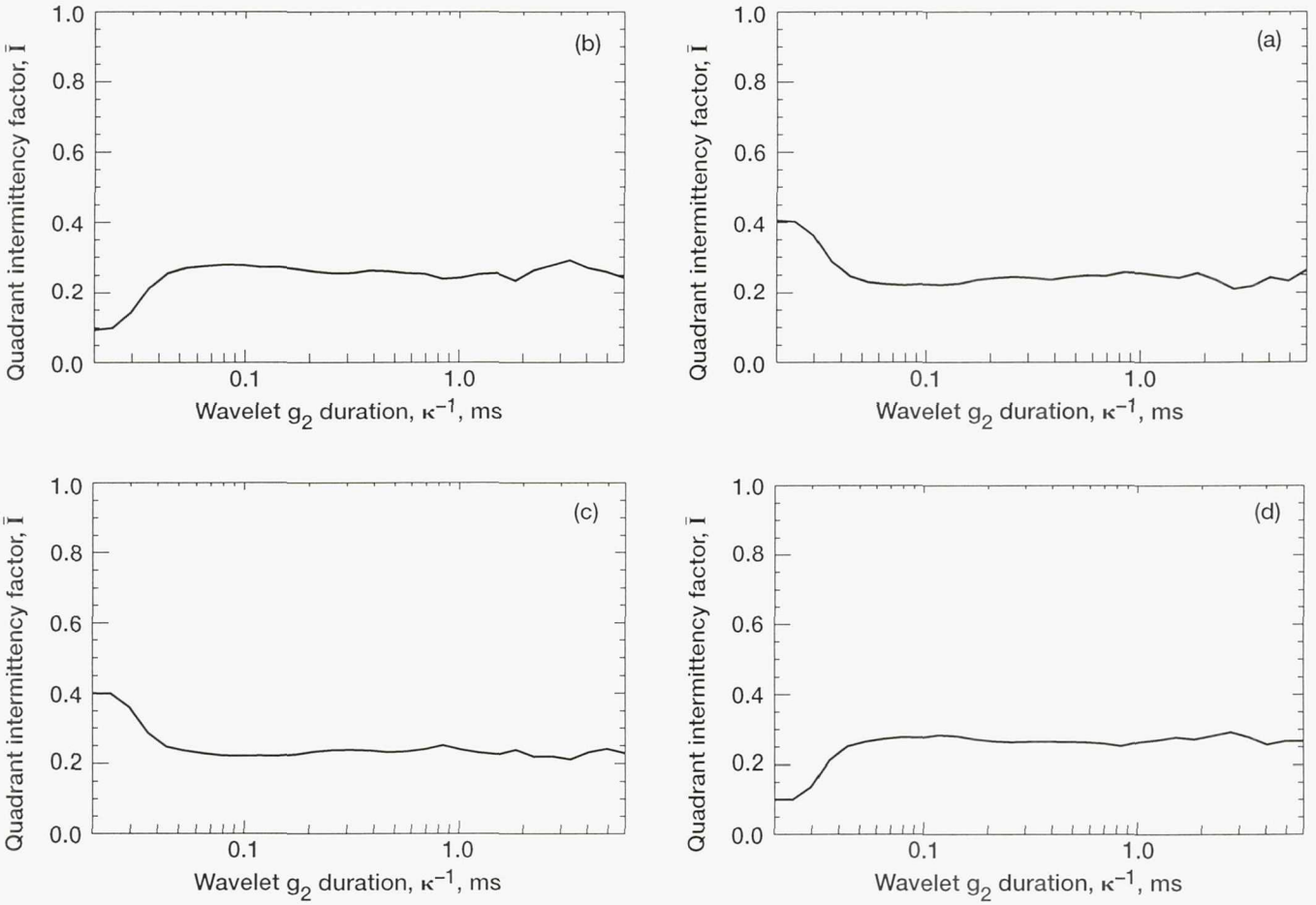

Figure 10.—Spectral quadrant intermittency factors measure fraction of the time at each duration that spectral contributions to fluctuations are in given quadrant. (a) Quadrant 1. (b) Quadrant 2. (c) Quadrant 3. (d) Quadrant 4.

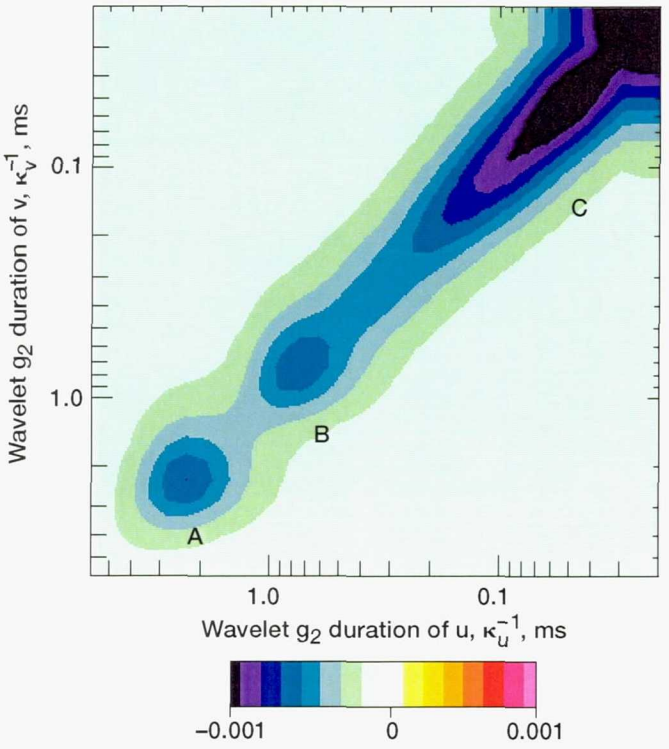

Figure 11.—Reynolds stress map showing filled contours of $\kappa_u\kappa_v\overline{U_1(\kappa_u,t)\ V_1(\kappa_v,t)}$ in m^2/sec^3 as function of durations κ_v^{-1} and κ_u^{-1}. Reynolds stress is associated with three narrow ranges of scales at durations of 2.5 ms (A), 0.6 ms (B), and around 0.05 ms (C). Noise is also in evidence in the 0.03-ms range.

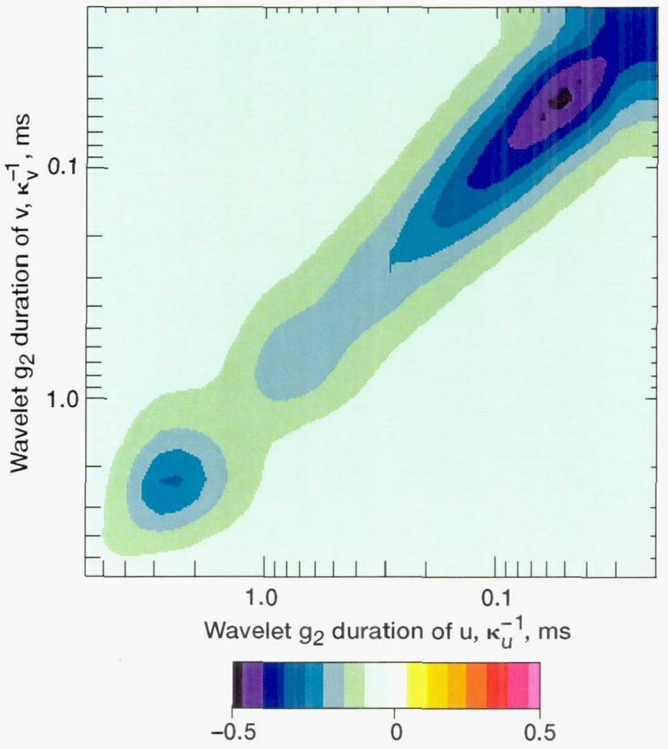

Figure 12.—Spectral correlation coefficients showing filled contours of $\kappa_u\kappa_v\overline{U_1(\kappa_u,t)\ V_1(\kappa_v,t)}/(U_1'\ V_1')$ as function of κ_u^{-1} and κ_v^{-1}.

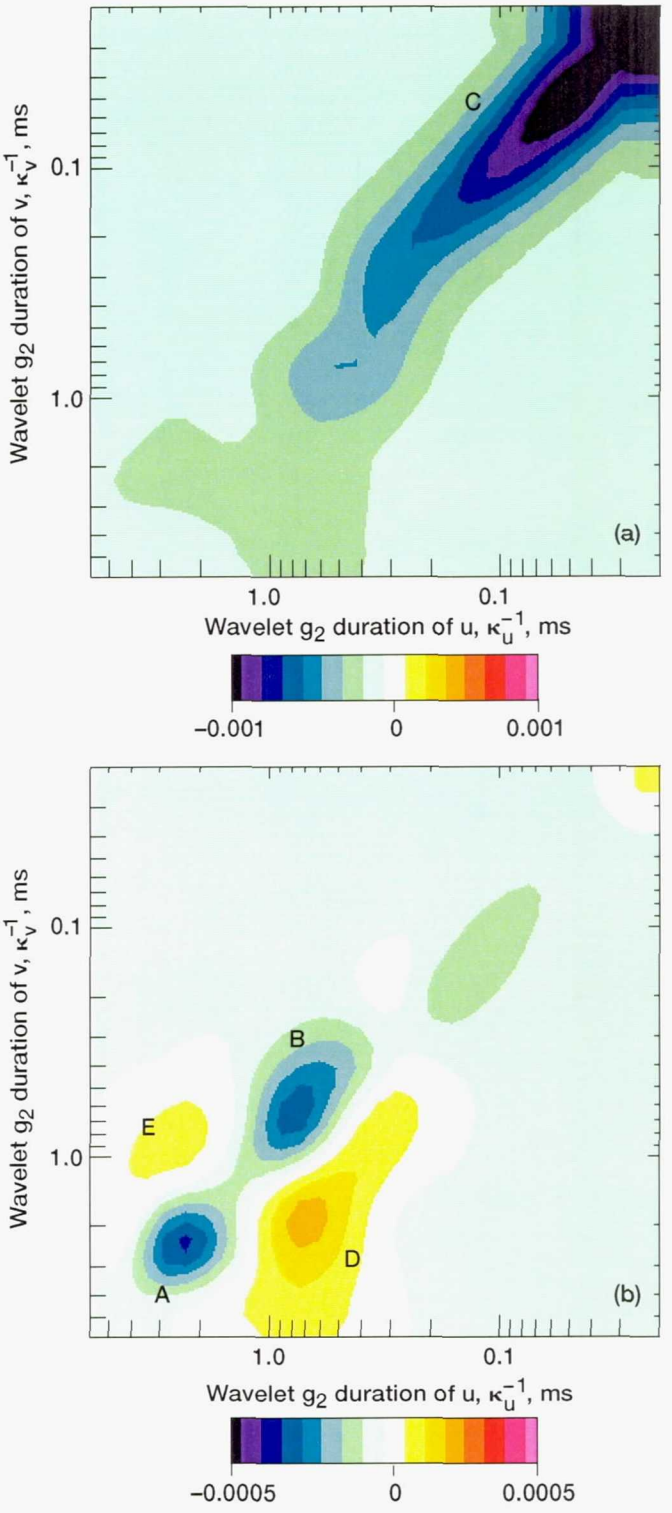

Figure 13.—Stress maps. (a) Turbulent-conditioned. (b) Laminar-conditioned. Three dominant scales noted in figure 11 are cleanly separated into a contribution from turbulent spots at small scales (C) and a double contribution from nonturbulent fluctuations at larger scales (A and B). Note regions of positive u-v correlations (D and E).

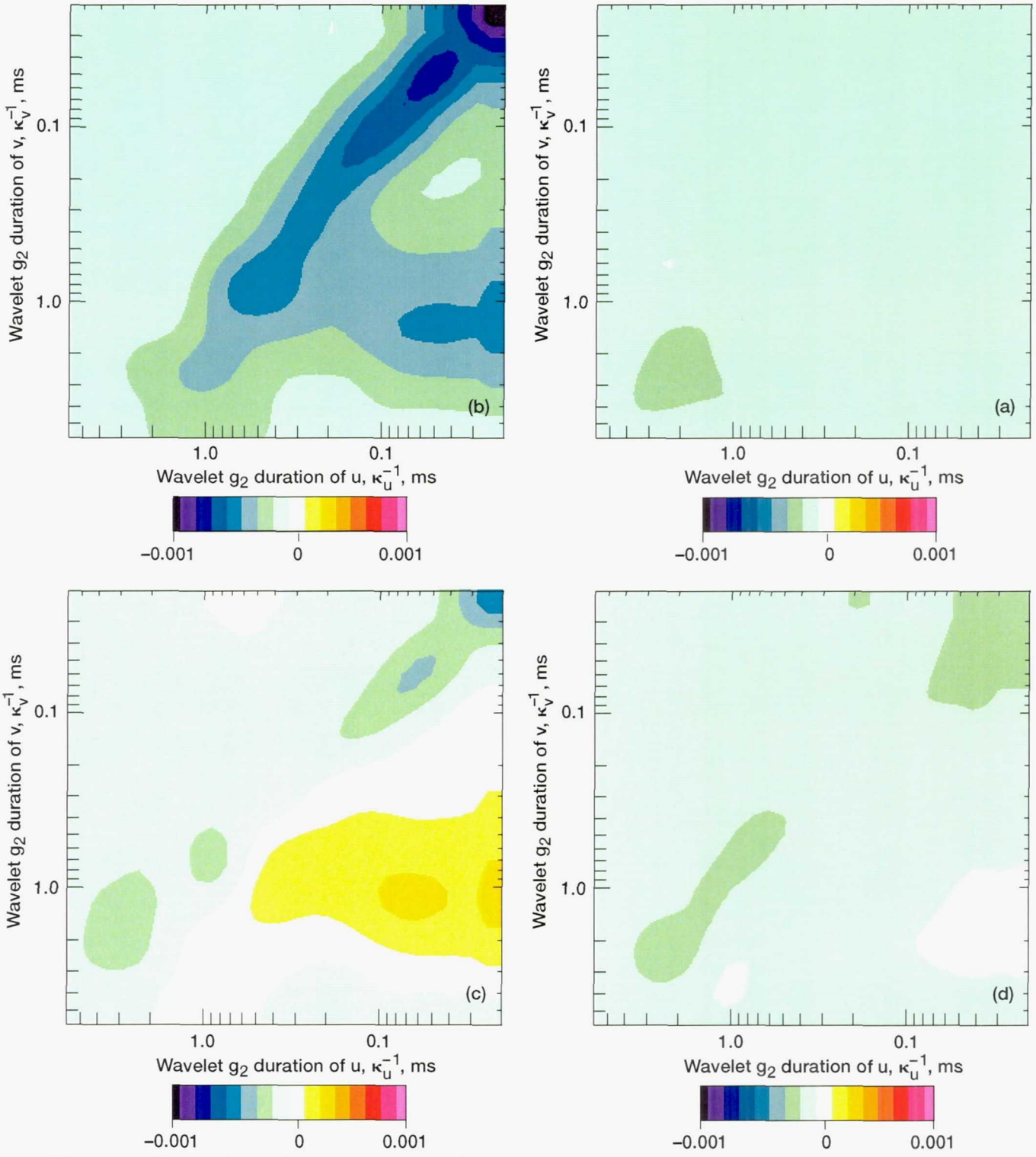

Figure 14.—Quadrant-conditioned stress maps. (a) Quadrant 1. (b) Quadrant 2. (c) Quadrant 3. (d) Quadrant 4.

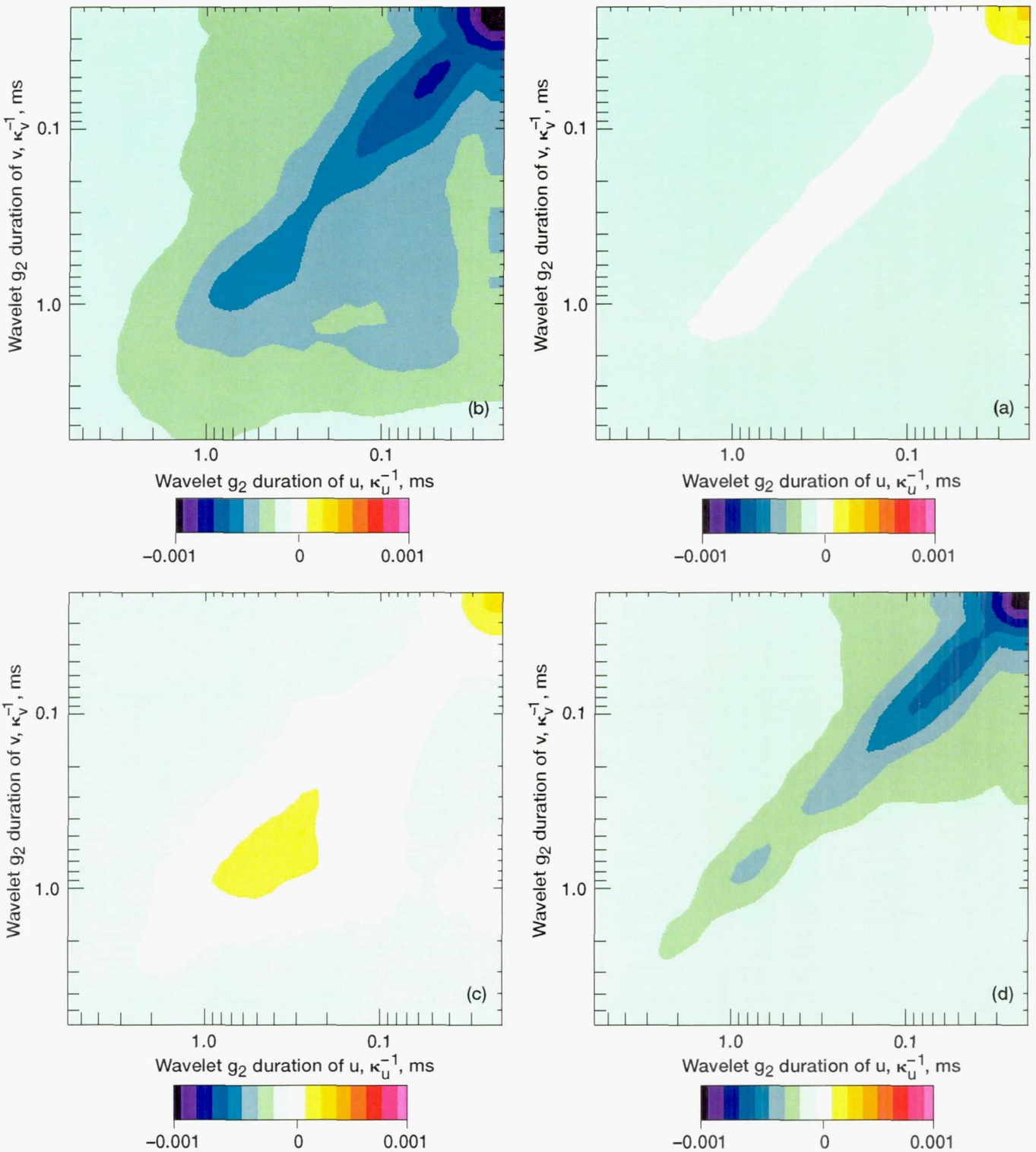

Figure 15.—Spectral quadrant-conditional stress maps. (a) Quadrant 1. (b) Quadrant 2. (c) Quadrant 3. (d) Quadrant 4.

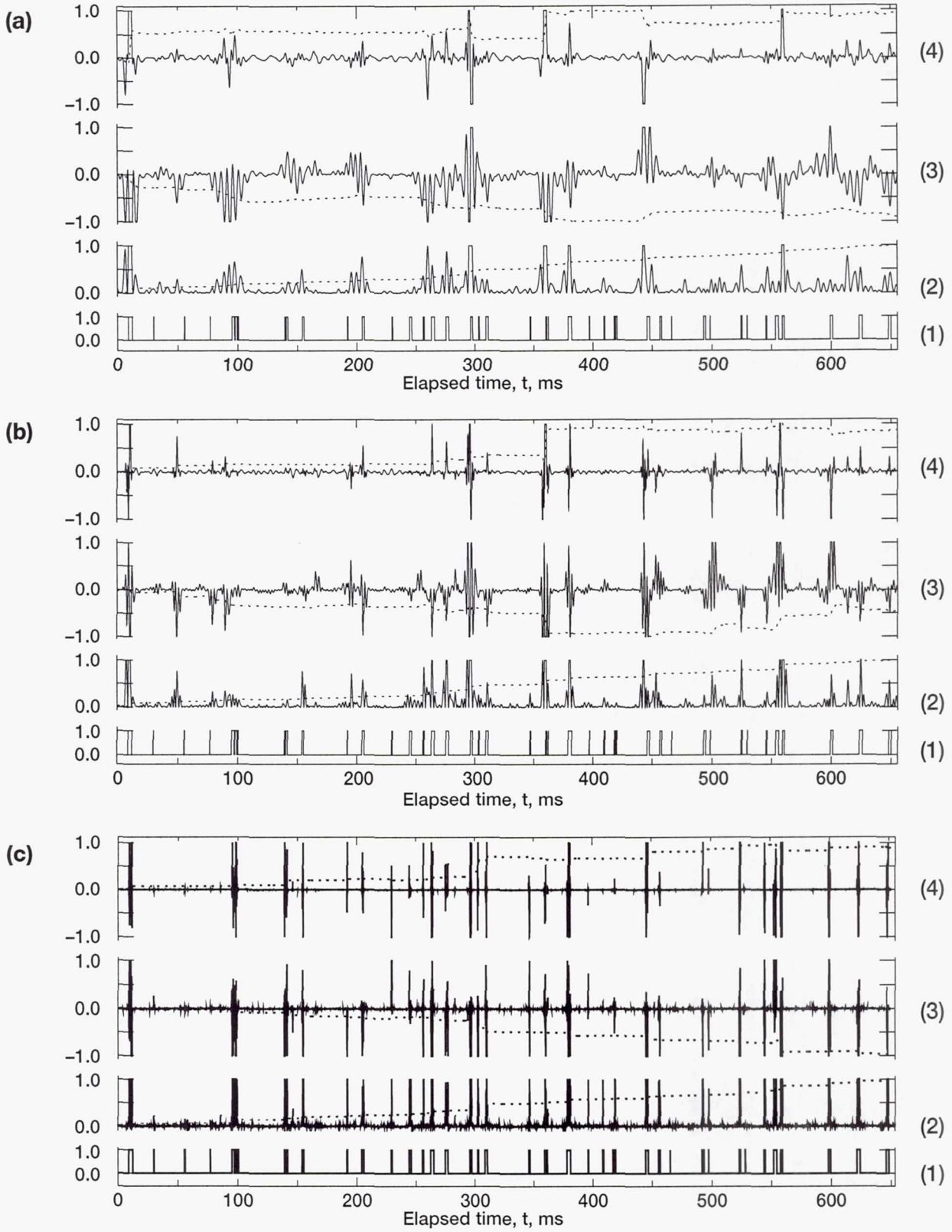

Figure 16.—Histories and spectral contributions to (1) turbulence indicator function, (2) energy, (3) Reynolds stress, and (4) energy flux. (a) Duration, 2.24 ms (0.11 kHz); wavelet mode n = 5. (b) Duration, 1.24 ms (0.2 kHz); wavelet mode n = 8. (c) Duration, 0.08 ms (3.2 kHz); wavelet mode n = 22. Note: solid lines are normalized histories (truncated at 3 standard deviations and normalized to unit variance); dashed lines are cumulative values (integrals of normalized history).

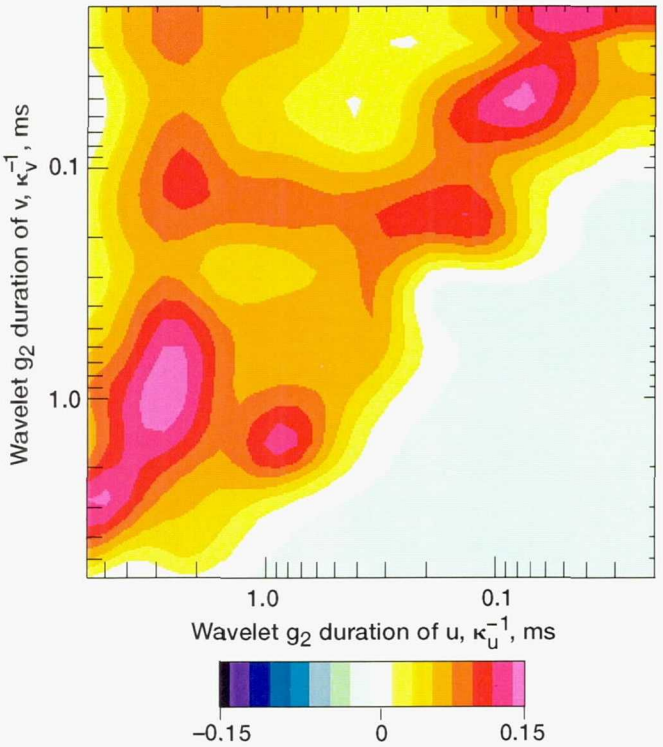

Figure 17.—Spectral distribution of transverse energy fluxes showing contour levels of $\kappa_u\kappa_v|\overline{u_2(\kappa_u,t)|^2 V_1(\kappa_v,t)}$ as function of κ_u^{-1} and κ_v^{-1}.

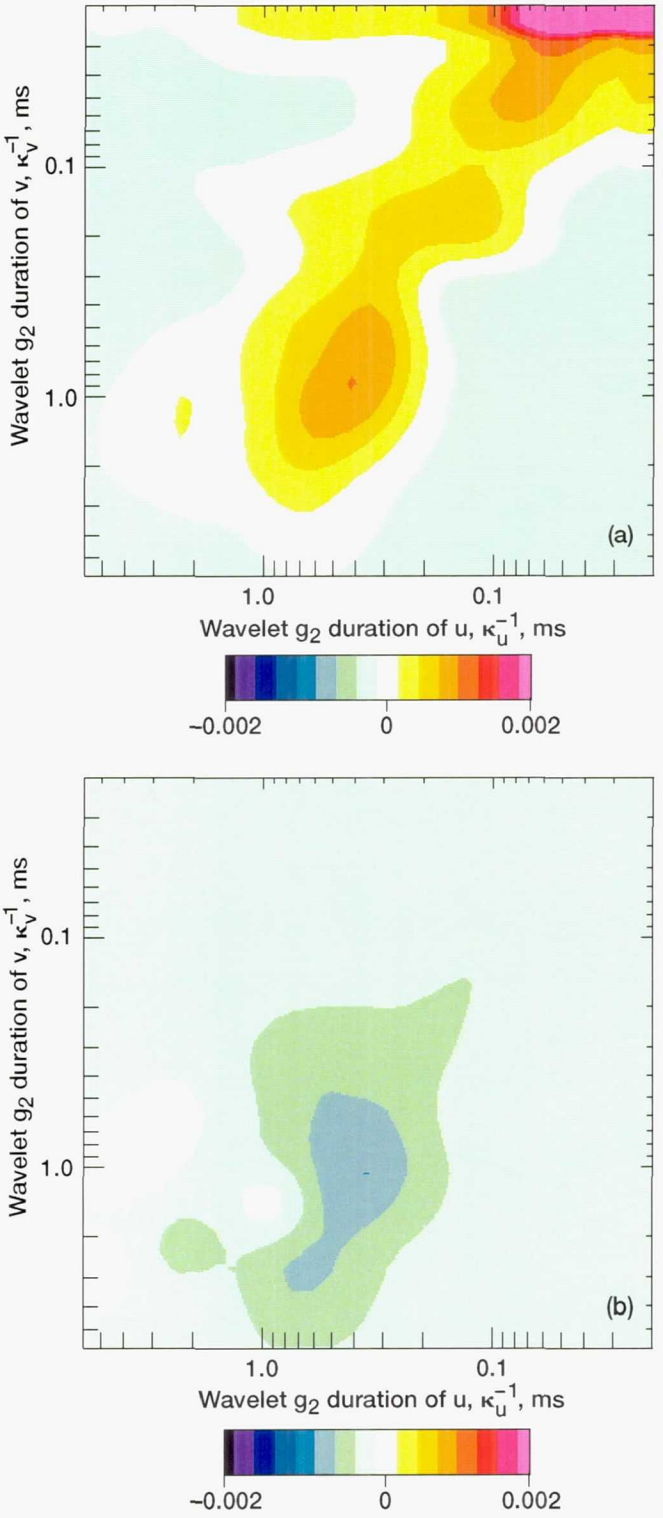

Figure 18.—Turbulent and laminar contributions to spectral flux map in figure 17. (a) Turbulent conditioned. (b) Laminar conditioned.

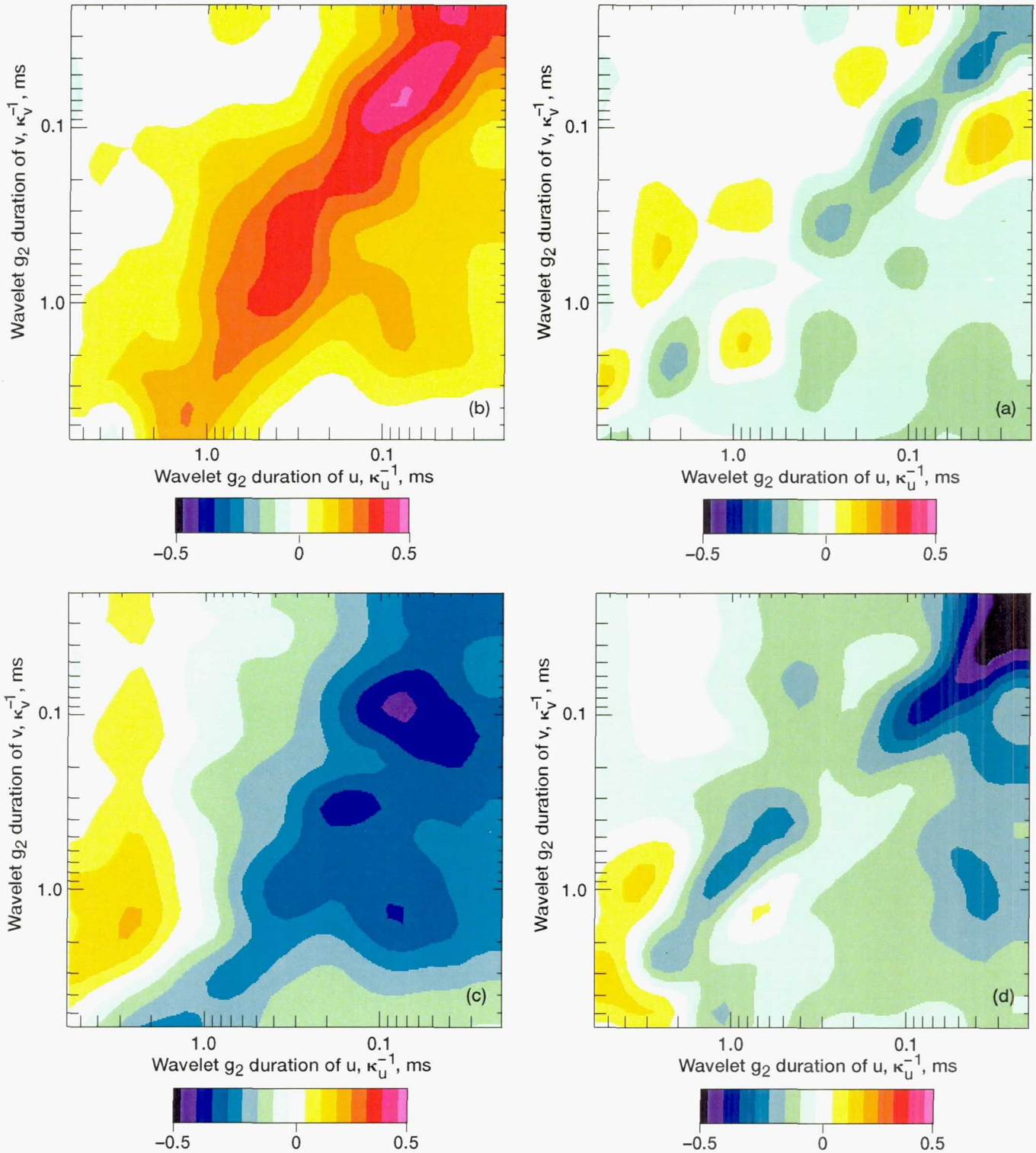

Figure 19.—Quadrant contributions to spectral flux map in figure 17. (a) Quadrant 1. (b) Quadrant 2. (c) Quadrant 3. (d) Quadrant 4.

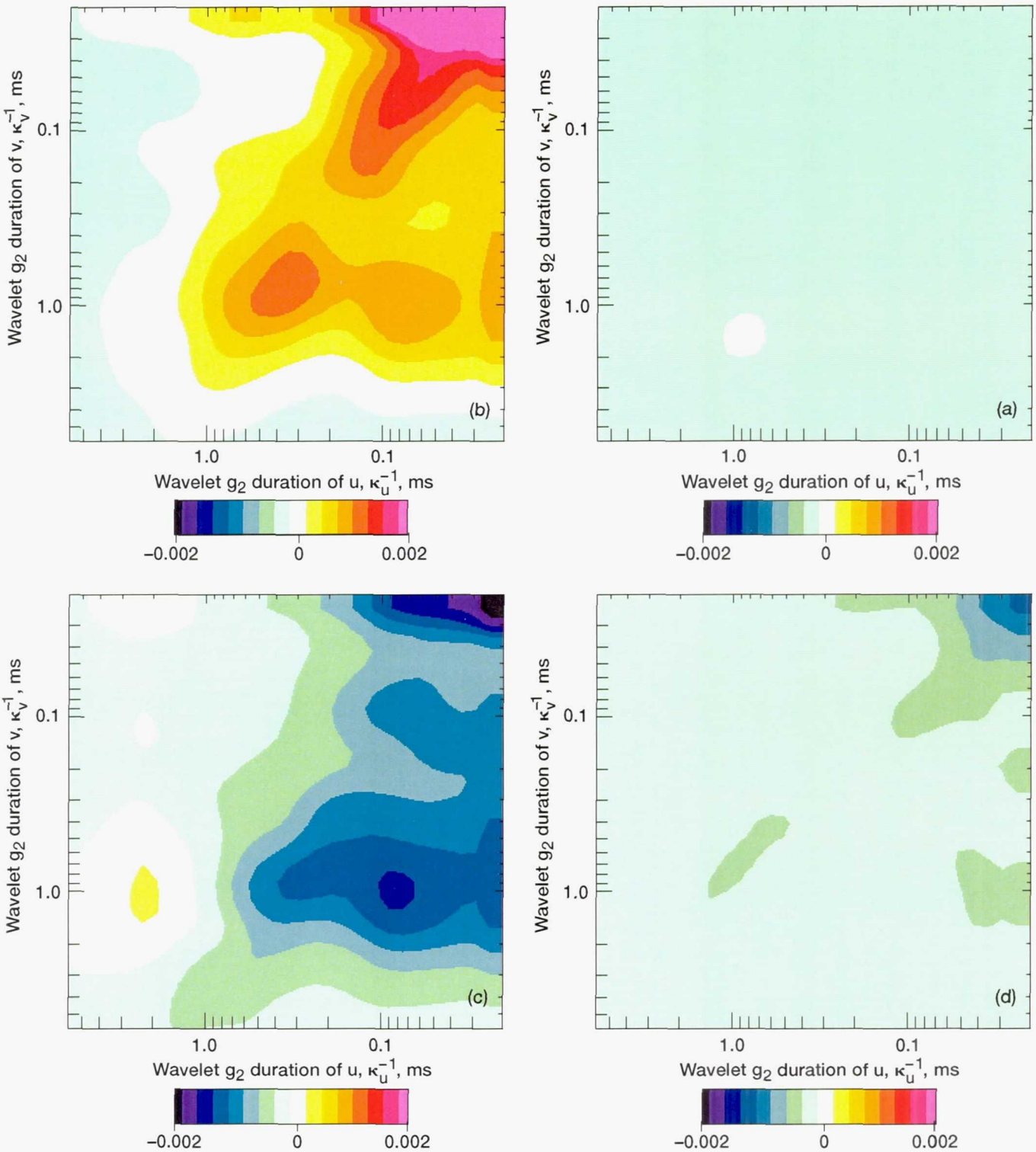

Figure 20.—Correlation coefficients corresponding to energy fluxes in figure 19. (a) Quadrant 1. (b) Quadrant 2. (c) Quadrant 3. (d) Quadrant 4.

REPORT DOCUMENTATION PAGE

Form Approved
OMB No. 0704-0188

1. AGENCY USE ONLY (*Leave blank*)	2. REPORT DATE	3. REPORT TYPE AND DATES COVERED
	December 1997	Technical Paper

4. TITLE AND SUBTITLE

Demonstration of Wavelet Techniques in the Spectral Analysis of Bypass Transition Data

5. FUNDING NUMBERS

WU–522–31–23

6. AUTHOR(S)

Jacques Lewalle, David E. Ashpis, and Ki-Hyeon Sohn

7. PERFORMING ORGANIZATION NAME(S) AND ADDRESS(ES)

National Aeronautics and Space Administration
Lewis Research Center
Cleveland, Ohio 44135–3191

8. PERFORMING ORGANIZATION REPORT NUMBER

E–9675

9. SPONSORING/MONITORING AGENCY NAME(S) AND ADDRESS(ES)

National Aeronautics and Space Administration
Washington, DC 20546–0001

10. SPONSORING/MONITORING AGENCY REPORT NUMBER

NASA TP–3555

11. SUPPLEMENTARY NOTES

Jacques Lewalle, Syracuse University, Syracuse, New York 13244–0003; David E. Ashpis, NASA Lewis Research Center; and Ki-Hyeon Sohn, University of Toledo, Toledo, Ohio 43606. Responsible person, David E. Ashpis, organization code 5820, (216) 433–8317.

12a. DISTRIBUTION/AVAILABILITY STATEMENT

Unclassified - Unlimited
Subject Categories: 34 and 02 Distribution: Standard

This publication is available from the NASA Center for AeroSpace Information, (301) 621–0390.

12b. DISTRIBUTION CODE

13. ABSTRACT ***(Maximum 200 words)***

A number of wavelet-based techniques for the analysis of experimental data are developed and illustrated. A multiscale analysis based on the Mexican hat wavelet is demonstrated as a tool for acquiring physical and quantitative information not obtainable by standard signal analysis methods. Experimental data for the analysis came from simultaneous hot-wire velocity traces in a bypass transition of the boundary layer on a heated flat plate. A pair of traces (two components of velocity) at one location was excerpted. A number of ensemble and conditional statistics related to dominant time scales for energy and momentum transport were calculated. The analysis revealed a lack of energy-dominant time scales inside turbulent spots but identified transport-dominant scales inside spots that account for the largest part of the Reynolds stress. Momentum transport was much more intermittent than were energetic fluctuations. This work is the first step in a continuing study of the spatial evolution of these scale-related statistics, the goal being to apply the multiscale analysis results to improve the modeling of transitional and turbulent industrial flows.

14. SUBJECT TERMS

Wavelets; Multiresolution; Bypass transition; Transition; Boundary layers; Turbulence; Conditional-statistics; Mexican hat wavelet; Intermittency

15. NUMBER OF PAGES

32

16. PRICE CODE

A03

17. SECURITY CLASSIFICATION OF REPORT	18. SECURITY CLASSIFICATION OF THIS PAGE	19. SECURITY CLASSIFICATION OF ABSTRACT	20. LIMITATION OF ABSTRACT
Unclassified	Unclassified	Unclassified	